OPTIMIZED FAN CONTROL IN VARIABLE AIR VOLUME HVAC SYSTEMS USING STATIC PRESSURE RESETS: STRATEGY SELECTION AND SAVINGS ANALYSIS

A Thesis

by

JOHN WILLIAM KIMLA

Submitted to the Office of Graduate Studies of
Texas A&M University
in partial fulfillment of the requirements for the degree of

MASTER OF SCIENCE

December 2009

Major Subject: Mechanical Engineering

OPTIMIZED FAN CONTROL IN VARIABLE AIR VOLUME HVAC SYSTEMS USING STATIC PRESSURE RESETS: STRATEGY SELECTION AND SAVINGS ANALYSIS

A Thesis

by

JOHN WILLIAM KIMLA

Submitted to the Office of Graduate Studies of
Texas A&M University
in partial fulfillment of the requirements for the degree of

MASTER OF SCIENCE

Approved by:

Chair of Committee,	David E. Claridge
Committee Members,	Charles H. Culp
	W. D. Turner
Head of Department,	Dennis L. O'Neal

December 2009

Major Subject: Mechanical Engineering

ABSTRACT

Optimized Fan Control in Variable Air Volume HVAC Systems

Using Static Pressure Resets:

Strategy Selection and Savings Analysis. (December 2009)

John William Kimla, B.S., Texas A&M University

Chair of Advisory Committee: Dr. David E. Claridge

The potential of static pressure reset (SPR) control to save fan energy in variable air volume HVAC systems has been well documented. Current research has focused on the creation of reset strategies depending on specific system features. As the commissioning process has begun to require the prediction of savings, knowledge of the extent to which various SPR control strategies impact fan energy has become increasingly important. This research aims to document existing SPR control strategies and utilize building data and simulation to estimate fan energy use.

A comprehensive review of the literature pertaining to SPR control was performed and the results were organized into a top-down flow chart tool. Based on the type of feedback available from a particular system, or lack thereof, this tool will facilitate the selection of a SPR control strategy. A field experiment was conducted on a single duct variable air volume system with fixed discharge air temperature and static pressure setpoints. Finally, an air-side model of the experimental system was created using detailed building design information and calibrated using field measurements. This model was used to estimate the fan energy required to supply the trended airflow data using fixed static pressure (FSP) and SPR control based on zone demand, system demand, and outside air temperature.

While utilizing trend data from November 1, 2008 to February 12, 2009, the FSP control of the experimental system was used as the baseline for ranking the energy savings potential of nine different forms of duct static pressure control. The highest savings (73-74%) were achieved using zonal demand based SPR control. System demand based SPR control yielded savings ranging from 59 to 76%, which increased when the duct sensor was positioned near the fan discharge and under similar zone load conditions. The outside air temperature based SPR control yielded savings of 65% since the experimental system supplied primarily perimeter zones. Finally, increasing the FSP setpoint from 2 to 3 inWG increased fan energy by 45%, while decreasing the setpoint from 2 to 1 inWG decreased fan energy by 41%.

DEDICATION

To my parents

ACKNOWLEDGEMENTS

I would like to especially thank Dr. David Claridge for his guidance and encouragement throughout the past few years. It was during his undergraduate class that I discovered my passion for this field and because of his patience and accessibility that I was able to complete this work. I would also like to thank Dr. W. Dan Turner and Dr. Charles Culp for their support during the course of this research. Thanks also go to Song Deng, Chen Xu, and Qiang Chen for providing the opportunity to join the Energy Systems Laboratory and develop my engineering skills.

The results of this project could not have been obtained without the support of Cory Toole, who arranged and collected the system trends, and was always available for discussion. In addition, I want to thank Michael Martine for his help in taking field measurements and Diane McCormick for facilitating the timely completion of this work. Finally, I wish to thank my dear friend, Arian Vistamehr, who provided constant support and motivation throughout my graduate studies.

TABLE OF CONTENTS

Page

LIST OF FIGURES

Page

Page

LIST OF TABLES

Page

1. INTRODUCTION

1.1 Background

1.1.1 Commercial Building Energy Consumption

A recent survey (EIA 2006) found there to 4,645 thousand commercial buildings (non-mall) with 64,783 million total square feet. According to the data, variable air volume (VAV) systems serve approximately 30% of this square footage. Commercial buildings account for 18% of the U.S. primary energy consumption (99.5 quads). The HVAC systems in these buildings account for approximately 31% of the primary energy consumed through space cooling (12.6%), heating (12.1%), and ventilating (6.7%) (NETL 2008). A study (Westphalen and Koszalinski 1999) based on building type, system type, and region information found that commercial building auxiliary HVAC equipment consumed 1.5 quads nationwide annually. In addition, 50% (219.8 billion kWh) of this energy came from building supply and return fans and 15% (65.9 billion kWh) was consumed by VAV systems.

1.1.2 Optimized VAV Systems

The most common method of supply fan control in VAV systems is closed loop proportional-with-integral (PI) control, which utilizes the pressure measured in the main supply duct. The fan output may be regulated using a variety of techniques; however, variable speed drives (VSDs) are commonly used due to their low energy consumption (ASHRAE 2007b). During periods of low load in VAV systems, terminal box dampers are forced to provide additional resistance to maintain the required airflow to each zone. A static pressure reset (SPR) may be utilized to reduce the duct static pressure, thus forcing the terminal box dampers to open, while maintaining the same airflow.

This thesis follows the style of *HVAC&R Research.*

Various SPR control strategies have been devised in an attempt to save fan energy during these conditions based on the type of system control (Federspiel 2005). ASHRAE Standard 90.1 (ASHRAE 2007a) states that "for systems with DDC [direct digital control] of individual zone boxes reporting to the central control panel, static pressure setpoint shall be reset based on the zone requiring the most pressure". The most common types of terminal box feedback used in commercial buildings include: damper position, airflow setpoint, or saturation signal (ASHRAE 2007b).

In addition to saving fan energy, this reset may reduce the number of hours the fan operates in the surge zone (Hydeman and Stein 2003), decrease noise levels, reduce the amount of leakage through the ductwork and terminal box dampers (Liu et al. 1998), and increase motor and fan bearing life (Rose and Kopko 1994).

1.2 Purpose and Objectives

The purpose of this research is to review the existing work related to SPR control and improve the procedures for SPR control selection and the understanding of the impact of SPR control on fan energy use. Energy management and control system (EMCS) trend data obtained during a field experiment along with simulation will be used in this analysis. The objectives of this research include:

- Create a methodology for assisting engineers in selecting the most energy efficient SPR control strategy given specific system features.
- Improve the understanding of the impact of different SPR control strategies on fan energy use.

1.3 Literature Review

This review is intended to document the methods to reset duct pressure based on system requirements, the attempts to model SPR control, and the important considerations when implementing SPR control in a building.

1.3.1 Methods to Reset Static Pressure Using Terminal Box Feedback

1.3.1.1 Airflow Based

Hartman (1989; 1993) introduced the Terminal Regulated Air Volume (TRAV) concept which directly controlled the speed of the supply fan using real time terminal box airflow requirements. This concept eliminated the need for a duct static pressure sensor and instead relied on the difference between the terminal box setpoint and measured airflows. A representative fan speed control algorithm was presented by Hartman (1995).

Englander and Norford (1992) proposed two control strategies to utilize terminal box DDC feedback to directly control the supply fan speed. All of the terminal box controllers were polled and an error signal was calculated based on the maximum or average difference between the setpoint and measured airflows. The energy saving potential of each SPR control strategy was verified using the simulation software HVACSIM+ (Clark 1985). When implementing SPR control in an actual building, it was recommended to use an inner loop to regulate the static pressure and an outer loop to reset the static pressure setpoint. The use of two loops would separate the control of the supply fan from the regulation of airflow and lead to an increase in system stability (Lorenzetti and Norford 1993).

1.3.1.2 Airflow Based Utilizing Static Pressure Sensor

Rather than calculate the difference between the setpoint and measured airflows for each terminal box, Warren and Norford (1993) programmed the terminal box controllers to trigger an alarm when they were unable to meet their required airflow. The number of alarms was used to

adjust the static pressure setpoint. Since data was only available during SPR control, a model was created to predict the amount of fan energy required under fixed static pressure (FSP) control using previously measured supply air velocity. The calculated savings ranged from 19 to 42% with the greatest savings obtained during periods of low airflow.

Tung and Deng (1997) supplied the same amount of airflow to two middle floors of an unoccupied building where one floor had FSP control and the other SPR control. The terminal boxes were pressure independent and electric heaters were used to simulate occupancy loads. The difference between the setpoint and measured airflows across all of the terminal boxes was summed to obtain a single error signal for controlling fan speed. When the electric heaters were turned on and the thermostats were set to 25°C, an average fan energy savings of 30% was observed after switching from FSP to SPR control. Once the thermostat settings were reduced to 23°C, the savings dropped to an average of 20%.

Lee and Chow (2004) were the first to investigate the impact of SPR control on thermal comfort and indoor air quality (IAQ) in an occupied building. A yearlong experiment was conducted on a single floor of an office building in which the fan control was alternated between FSP and SPR control on a daily basis. Since the position of each terminal box damper was unavailable, the SPR control was based on the number of boxes requiring their design airflow. The SPR savings were found to increase up to 23% with decreasing outside air temperature. The measured savings were extended to the remaining floors of the building to obtain an overall annual fan energy savings of 8 to 9%. Comfort complaints and return air CO_2 levels were monitored during this period and no evidence was found that SPR control negatively impacted occupant comfort or IAQ.

The trim and respond SPR control method (Taylor 2007; Hydeman and Stein 2003; Hartman 1995) steadily reduces the duct static pressure setpoint until one or more of the terminal

boxes indicate that more pressure is needed to maintain the required airflow. Once the number of boxes exceeds a threshold value, the controller will increase the setpoint a small amount. This method circumvents common stability problems associated with PID control by enabling a separate response time for increasing and decreasing the static pressure setpoint. In addition, this method may be applied to demand indicators other than airflow such as damper position.

1.3.1.3 Damper Position Based

The use of terminal box damper position as a means of resetting duct static pressure was introduced by Rose and Kopko (1994). During a brief test the static pressure setpoint was manually reset, while monitoring all of the terminal boxes, such that one damper remained 100% open. This procedure yielded an estimated fan energy savings of 50%.

Haasl et al. (2001) proposed that all terminal boxes be polled every five minutes and the static pressure setpoint be adjusted between a minimum and maximum value to maintain at least one terminal box damper 95% open. Song et al. (2003) modified this type of SPR control by varying the minimum setpoint based on the variable frequency drive (VFD) speed (30 to 70%). Pang et al. (2006) polled each terminal box every twenty minutes and adjusted the setpoint based on the maximum damper position using a 85 to 95% dead band.

1.3.2 Methods to Reset Static Pressure without Using Terminal Box Feedback

1.3.2.1 Airflow Based

Rose and Kopko (1994) proposed a SPR control strategy for pneumatically controlled terminal boxes. This method used the ratio of measured static and velocity pressures, which remains constant for a given flow rate, as an indication of changing system resistance. This strategy was tested by installing two pressure sensors four duct diameters downstream of the air handling unit (AHU) and modifying the control programming. The fan speed was modulated to maintain an experimentally determined pressure ratio of ten, which was found to correspond to

an average damper position of approximately 50% open. The result was an average reduction in fan speed from 40 to 25 Hz during the winter.

Liu (2002) developed the concept of Variable Speed Drive Volumetric Tracking (VSDVT) for VAV systems. To avoid inaccurate airflow measurements, a fan airflow station (FAS) was created to calculate airflow using measured fan speed and fan head. Since pressure loss is proportional to the square of the flow rate under turbulent flow conditions, the duct static pressure setpoint may be calculated using this airflow. A modified version of this concept addressed system stability by accounting for the system load distribution profile using a load factor that increases with zone load ratio (Liu and Liu 2008; Wu et al. 2007).

Liu et al. (2002) recommended that the static pressure setpoint be linearly reset as a function of system airflow. In cases where the total airflow is not measured, the use of VFD speed is recommended. A case study demonstrated that resetting the static pressure setpoint based on VFD speed saved about 68 to 75% of the annual fan power.

1.3.2.2 Outside Air Temperature Based

Zheng et al. (2007) stated that linearly resetting the static pressure setpoint based on outside air temperature was an effective control strategy for envelope dominated buildings. The energy savings is heavily dependent on the minimum airflow setting and the outside air temperature range. This type of control has been implemented in a variety of building types (Dong et al. 2005; Evans et al. 2005; Liu et al. 1998, 2000; Martinez et al. 2007; Napper et al. 2007; Turner et al. 2003; Zeig et al. 2007; Zhu et al. 2001). In each of these cases, the static pressure setpoint was linearly reset between experimentally determined minimum and maximum setpoints between outside air temperatures of 50 and 90°F.

1.3.3 Model Driven Static Pressure Reset Strategies

The concept of model based predictive control was introduced by Goswami (1986) and Okada et al. (1992). Ahmed (2001) applied this concept to the control of large HVAC systems and Kalore et al. (2003) and Cascia (2007) automated the process for use in actual buildings. The application of this method requires access to a simple schematic of the duct system and the ability to collect test data. This data is used to create a model of the system by calculating the pressure loss coefficients for each duct section and terminal box. Once the building EMCS receives the airflow setpoint for each terminal box, the model will first calculate the airflow in each duct segment and then the static pressure requirement for each terminal box. The maximum requirement is selected as the fan static pressure setpoint. This method was implemented in three case studies where AHUs served 4, 9, and 55 terminal boxes. For each case, the static pressure sensor was located near the fan discharge and the reported fan energy savings over a nine month period compared to FSP control were 50, 38, and 30% respectively.

Federspiel (2005) used an experimentally derived model to dynamically identify the critical supply duct pressure. This pressure is defined as the point between the starved and controlling modes. The starved mode occurs when one (or more) terminal box damper is 100% open and not meeting the load, and the controlling mode occurs when all of the terminal boxes are meeting the load. This procedure is called Infer Critical Information about Terminals (InCITe) and laboratory and field tests have confirmed its ability to predict the critical fan pressure within ±6.5% and keep the flow within 3% of that required to maintain space temperature. This reset requires the measurement of supply duct static pressure and flow rate, is independent of sensor location, and takes into account duct leakage.

1.3.4 Modeling SPR Control

Wang and Burnett (1998) created a steady-state system model using component flow resistances derived from field measurements and a fan curve based on design data. An ideal controller was used to modulate the static pressure setpoint such that the critical terminal box damper remained 100% open while providing the required amount of airflow. The effect of load distribution on SPR performance was investigated by simulating two load scenarios. The first scenario had an evenly distributed load across all of the terminal boxes, and the second scenario had a maximum zone load that was 20% higher than the average load. It was concluded that evenly distributed loads resulted in an additional 3 to 9% savings when comparing SPR to FSP control.

Liu et al. (2007a) modeled a single duct system with one terminal box and an airflow based SPR control strategy. The model was used to analyze the impact of SPR control on both fan and thermal energy savings, while taking into account duct leakage, for numerous building control scenarios. According to the simulation results, fan energy savings increased from 15 to 50% as duct leakage increased from 0 to 30%. The performance of the system model was tested using an outside air temperature based load function. A 32% reduction in annual fan energy usage was calculated for a system with unsealed rectangular metal ductwork and pressure independent terminal boxes (Liu et al. 2007b).

Zheng et al. (2007) analyzed the performance of an idealized SPR control strategy based on terminal box damper position. The system model was based on actual duct dimensions and terminal box airflows obtained through building simulation. A flow coefficient was derived for each duct section and the pressure required to provide airflow to each zone was calculated when the terminal box damper was 100% open. On an hourly basis from 7:00 to 19:00, the maximum required terminal box pressure was selected as the fan static pressure setpoint. When the fan

energy savings were averaged over the twelve hour period, damper based SPR control was found to have the highest potential followed by airflow and outside air temperature based resets.

Khoo et al. (1997) simulated FSP and demand based SPR control on both radial and duct loop VAV system configurations. Since the loads were assumed synchronous (constant across all of the zones), SPR control was approximated using the ideal cubic relationship between airflow and power. The switch from FSP control with the sensor located near the fan discharge to ideal SPR control (sensor position irrelevant) resulted in a maximum fan energy savings of 19% for radial systems and 10% for duct loop systems. It was also demonstrated that duct loop systems require less fan energy than radial duct systems to supply the same amount of airflow (Levermore 2005).

Federspiel (2003) modeled a built-up AHU to demonstrate the benefits of the Energy-efficient Air-handling control StrategY (EASY) while varying the supply airflow from 0 to 100%. The simulation results indicated that the SPR control strategies based on critical damper position and airflow had a larger impact on VAV system power consumption than optimized damper and return air fan control strategies. It was calculated that FSP control consumed an average of 0.623 W/sf across the range of airflows, whereas the resets based on damper position and airflow consumed an average of 0.445 W/sf and 0.464 W/sf respectively.

Hydeman and Stein (2003) used trended 15 minute supply airflow and fan head data obtained during FSP control to estimate the energy savings potential of SPR control. It was determined that SPR control could reduce fan energy usage by up to 50% assuming an ideal system curve.

Lorenzetti and Norford (1993) collected ten days of data for both FSP and SPR control to derive a typical day profile based on the hourly averaged measurement of static pressure and fan motor power. A direct comparison of the area under each curve provided an estimated

savings of 39% assuming similar load conditions. It was concluded that the energy savings resulting from SPR control was dependent on the amount of system airflow and on the relative distribution of air supplied to each terminal box.

1.3.5 Considerations When Implementing Static Pressure Reset Control

1.3.5.1 Sensor Location

The location of the static pressure sensor under SPR control is less critical than FSP control (ASHRAE 2007b). In general, moving the sensor closer to the fan prevents the need to install a sensor in each branch and utilizes the larger velocity pressure signal (Lorenzetti and Norford 1993). In the case of direct fan speed control based on terminal box airflow requirements a static pressure sensor is not required.

1.3.5.2 Terminal Box Component Failure

Wei et al. (2000; 2004) explained that SPR control based entirely on damper position may experience a loss in performance due to various system faults (e.g. stuck damper, leaking reheat valve, undersized terminal box, etc.). The proposed Integrated Damper and Pressure Reset (IDPR) method integrates a secondary control loop into the existing fan speed control based on zone demand. The output of the secondary loop based on outdoor air temperature, supply fan speed, or time of day is compared to the primary loop output and the lower value will be used to control the fan speed.

Local thermostat calibration issues may cause SPR control strategies based on damper position to default to their maximum settings. These problems may be avoided by using the second or third most open damper (Wang and Burnett 1998; Wang 1999).

1.3.5.3 Control Loop Parameters

When resetting duct static pressure using zonal feedback, the fan and duct static pressure controllers should react slower than the terminal box controllers to ensure stable operation

(Englander and Norford 1992). Additional system stability may be obtained without extensive loop tuning by utilizing a wide static pressure throttling range (Warren and Norford 1993) or limiting the amount of fan speed variation allowed in a given period of time (Tung and Deng 1997).

1.3.5.4 Use of EMCS Trend Data to Evaluate System Performance

Recorded EMCS data may be used to identify efficiency and performance problems as well as establishing static pressure requirements in HVAC systems (Brightbill and Rutt 1998). Stum (1998) provided recommendations regarding value stream and change of value (COV) trends as well as sampling rates. Salsbury and Singhal (2003) discussed the issues that arise when digital output from a control system is used to derive real system behavior. Signal quantization (rounding of signal values), which is compounded when COV trends are used, may have the effect of misrepresenting the behavior of recorded data. In addition, sampling rates of one second or faster were recommended for highly dynamic data points such as static pressure.

1.3.6 Summary of Literature Review

The literature review presents several case studies demonstrating the potential of SPR control to reduce fan energy usage. It has been shown that this method of control may be implemented with and without terminal box feedback using a variety of techniques. Despite these efforts no work has been done to summarize these techniques based on system requirements.

To estimate the savings potential of these techniques several system models have been created. Although some of these models were intended to represent actual systems, through the use of building duct dimensions and supply fan design data, all of the loads were based on simulation. The amount of fan energy savings resulting from SPR control has also been calculated using trended data; consequently, the limitations of this approach have been reviewed.

These efforts have all failed to incorporate trended data in the simulation of built systems under various methods of SPR control.

2. PROJECT APPROACH

The goal of this research is to aid engineers in recommending SPR control as part of the commissioning process. This research addresses this goal through two primary objectives: (1) create a methodology for assisting engineers in selecting the most energy efficient SPR control strategy given specific system features and (2) improve the understanding of the impact of different SPR control strategies on fan energy use.

2.1 SPR Control Strategy Selection Chart

The SPR techniques identified in the literature review are summarized in Figure 1. This top-down flow chart may be used to identify the techniques applicable to a specific system based on the availability of terminal box feedback and measured data. The indented boxes indicate a subtle variation in technique. This process identified three major categories of SPR control: zonal demand based, system demand based, and use of indirect measurements often related to building load such as outside air temperature.

For systems with terminal box feedback, damper position and airflow are common indicators of demand; however, there are several alternatives such as damper command and low airflow alarm. When damper position is available, the ideal scenario is to reset the static pressure setpoint between a minimum and maximum value such that one damper remains 100% open. In practice, values less than 100% should be used since PID loops require there to be an error on both sides of the setpoint. When the minimum static pressure requirement has not been experimentally determined, increased savings may be obtained by resetting this setpoint according to fan speed.

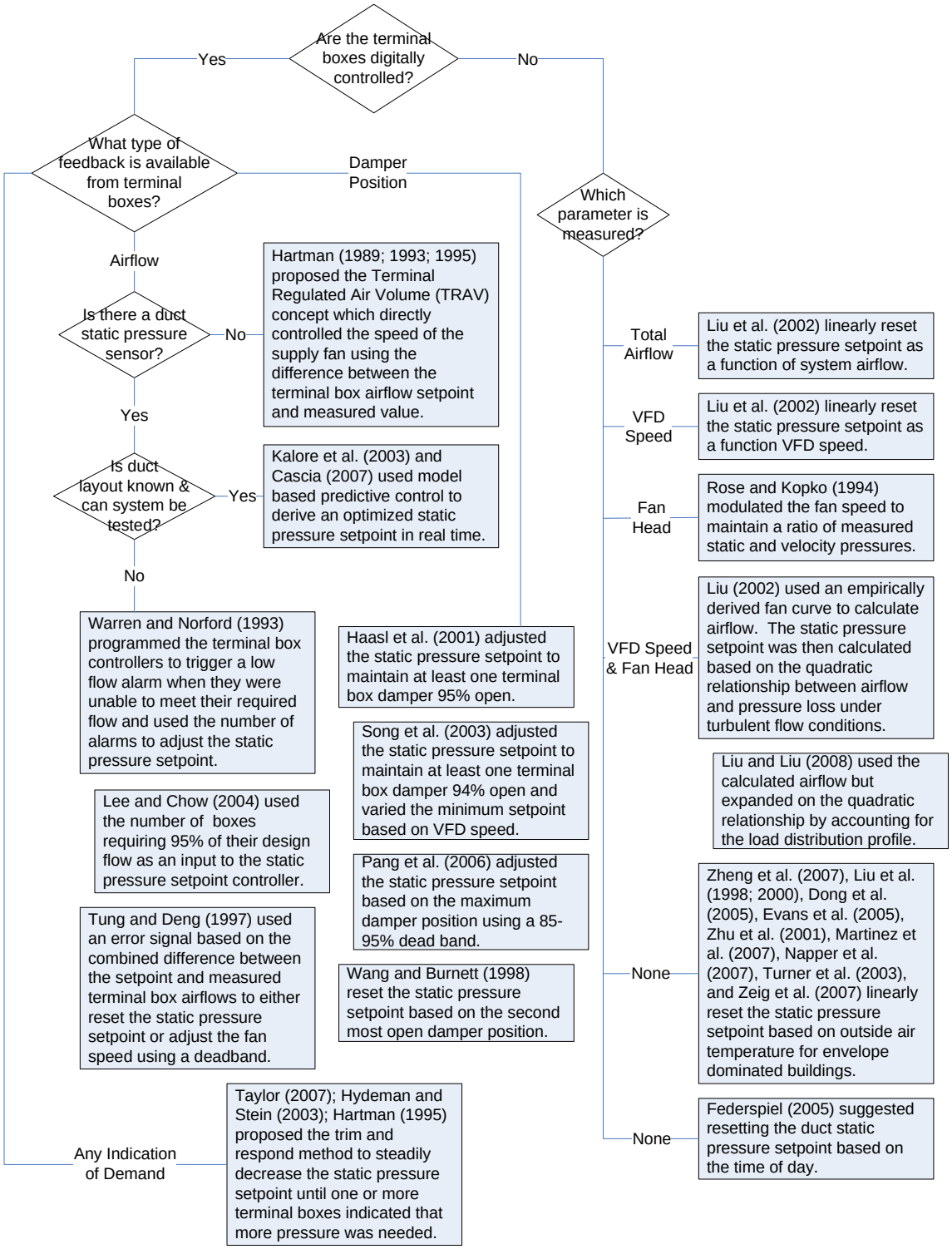

Figure 1. SPR control strategy selection flow chart

To increase system stability without extensive loop tuning a dead band may be implemented. For example, if the critical zone terminal box damper position is between 85 and 95% no change is made to the setpoint. For systems with a large number of terminal boxes, where there is a high probability of mechanical failure, the static pressure PID loop may be activated once a certain number of terminal boxes exceed the maximum allowable damper position. This strategy has the potential to prevent unnecessarily high setpoints; however, a proper balance must be maintained between building requirements (space temperature and ventilation) and control loop performance. When a static pressure sensor is not installed, terminal box airflows may be used to directly control the fan; however, it has been documented that separating the control of the supply fan from the regulation of airflow will result in an increase in system stability.

Model based control has been implemented on systems with static pressure sensors; however, knowledge of the duct layout and software to generate the model are required. In cases where this is not possible, several strategies utilizing the difference between the terminal box setpoint and measured airflows have been proposed. A common strategy is to increase the static pressure setpoint when a certain number of terminal boxes indicate that the airflow is sufficiently below setpoint. Similar to the aforementioned damper based control, building space temperature and ventilation requirements must be considered when implementing this strategy.

Since the trim and respond method does not rely on PID logic, different reset rates may be used for increasing and decreasing the static pressure setpoint. This ensures that the setpoint may be decreased slowly enough to allow the system to respond in a stable manner, while increased quickly enough to respond to changes in load.

For systems lacking DDC terminal boxes, several strategies related to system demand have been proposed. Depending on the type of feedback available related to the supply air fan,

the total airflow (measured or calculated), head, or VFD speed may be used to reset the static pressure setpoint. Finally, resets based on measurements often related to building load such as outside air temperature or time of day may be implemented when there is no feedback available from the system.

2.2 Methodology for Estimating Fan Energy

The fan power required for various types of duct static pressure control was estimated using a combination of building experimentation and simulation. The purpose of the experiment was to collect trend data for a typical system operating under FSP and SPR control. In parallel, a model of the experimental system was created using building design information and calibrated using field measurements. A portion of the trend data was selected as an input to the calibrated model and the fan energy performance was simulated for a representative SPR control strategy based on zonal demand, system demand, and outside air temperature. The simulated energy includes the inefficiencies associated with the fan, v-belt, motor, and VFD.

3. OVERVIEW OF FIELD EXPERIMENT

3.1 System Description

The Jack E. Brown (JEB) building is located on the main campus of Texas A&M University and was constructed in 2004. This modern building was selected because all of its components are accessible through the campus EMCS program operated by Siemens APOGEE. The single duct VAV system selected is summarized in Table 1. The discharge air temperature is fixed and the supply fan speed modulates to maintain a FSP setpoint, which is measured approximately 2/3 down one of the main supply duct branches. Figure 2 illustrates the layout of the ductwork as well as the location of the duct static pressure sensor.

This AHU supplies conditioned air via eleven DDC terminal boxes. Nine of these zones serve perimeter office space with parallel fan powered reheat terminal boxes, and two serve interior electrical and communications rooms with series volume only terminal boxes. Additional information regarding the airflow setpoints for these terminal boxes is provided in Appendix A.

Table 1. Overview of the experimental AHU

Designation	AHU 5-1
Type	Single duct VAV with VSD
Discharge air temperature setpoint	56°F
Static pressure setpoint	2 inWG
Design airflow	7,500 CFM
Conditioned area	7,500 ft^2

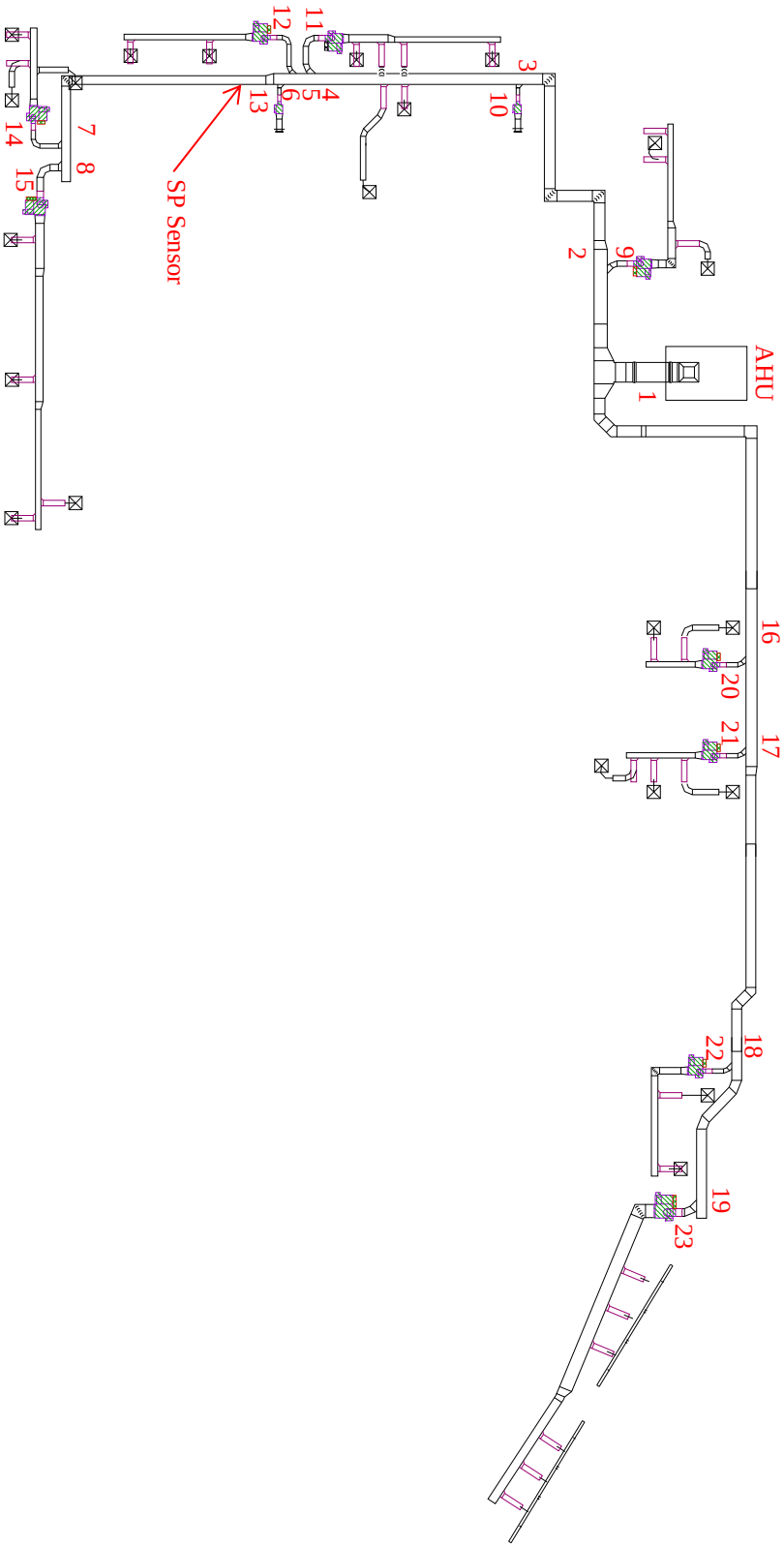

Figure 2. Jack E. Brown building AHU 5-1 duct layout

3.2 Data Collection

A record of the system performance was maintained by trending the points specified in Table 2. The building EMCS was used to perform this operation by automatically recording a "snapshot" of 58 control points every 15 minutes beginning November 1, 2008. At the time of this experiment, control points for total AHU supply airflow and VFD power were not available.

Table 2. EMCS point names trended during AHU experiment

AHU	**Terminal Box**
Fan speed	Zone temperature
Duct static pressure	Zone temperature setpoint
Duct static pressure setpoint	Supply air (from AHU) damper position command
Cooling coil temperature	Supply airflow (from AHU)
Cooling coil valve position	Reheat valve position command

3.3 Control Modifications

Beginning on March 2, 2009, the AHU control programming was modified to continuously identify the most open terminal box damper position. The static pressure PID loop compared the most open damper position to a setpoint of 85% and output a static pressure setpoint to minimize the loop error every 3 seconds. The VFD PID loop compared the static pressure measured in the duct to the setpoint every second and output a fan speed (20 to 100%) to minimize the static pressure error.

3.4 Review of Trended Data

3.4.1 Period of FSP Control

The individual terminal box airflows and VFD speed were trended with a sampling rate of 15 minutes, while the supply fan VFD modulated to maintain a FSP setpoint, from November 1, 2008 to March 2, 2009. An unknown change to the system was found to have occurred on February 13, 2009, which led to the increase in VFD speed shown in Figure 3. Since a

measurement of total supply airflow was unavailable, the individual terminal box airflows were summed to obtain this value. This sum was averaged on an hourly basis and the fraction of design airflow was calculated based on the design value of 7,500 CFM documented in the building design drawings.

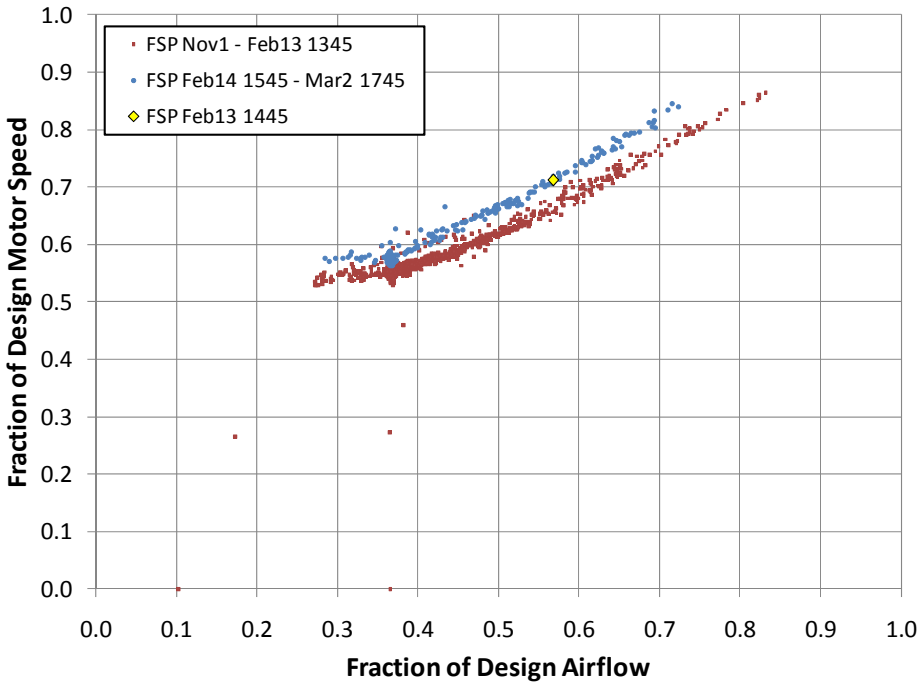

Figure 3. Hourly averaged ratio of design motor speed trended during FSP control

3.4.2 Period of SPR Control

The supply fan VFD modulated to maintain a dynamically reset static pressure setpoint beginning March 2, 2009. The hourly averaged trended VFD speeds were converted to fraction of power using the ideal cubic relationship in Figure 4. A review of the 15 minute data revealed that the maximum airflows frequently corresponded to the lowest VFD speeds (out-of-phase) during periods of low load. Since VFD speed was used to calculate power, anytime the supply airflow was at a maximum when the VFD speed was at a minimum, points would appear below

the ideal curve. When the opposite behavior was observed, fan power values at or above the FSP points would appear.

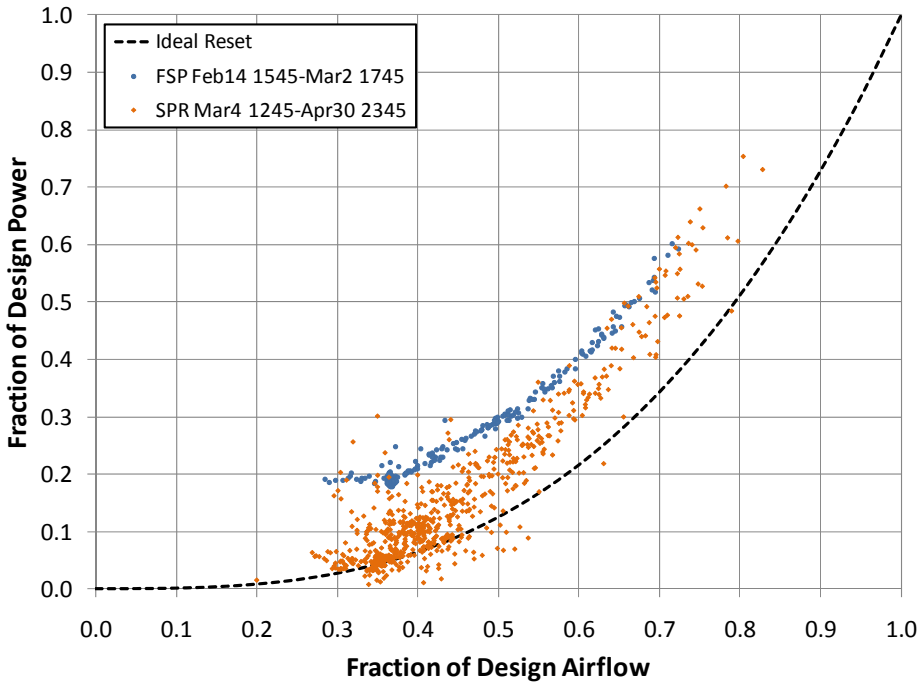

Figure 4. Hourly averaged ratio of ideal power for trended FSP and SPR control

The accuracy of the 15 minute data was evaluated using the EMCS COV trend option. The terminal box airflows, duct static pressure, and VFD speed were recorded if the point value change exceeded 1 CFM for airflow, 0.1 inWG for static pressure, and 1% for VFD speed. The COV data revealed that the system airflow and VFD speed were always in-phase. This finding verified that 15 minute trend data does not accurately describe the performance of systems controlled by dynamic setpoints. It was concluded that the 15 minute data appeared out-of-phase because the amount of time required by the EMCS to record each trend point exceeded the VFD loop time.

3.4.3 Selection of Data for Model Simulation

The available 15 minute trend data can be divided into three periods: (1) FSP, (2) FSP with unknown change to the system, and (3) SPR. Due to the dynamic nature of SPR control, it was confirmed that a 15 minute trend interval leads to a misrepresentation of system behavior. Furthermore, the data corresponding to FSP control after the system change occurred amounted to less than one month of data. Consequently, the first period of trend data was selected as an input to the system model.

4. MODEL DESCRIPTION

An air-side model of the experimental AHU was created based on the information provided in the building design drawings and the procedure outlined in Figure 5. The trended terminal box airflows selected were used to calculate the amount of airflow throughout the system and the corresponding pressure losses through each duct section and fitting. Once the static pressure sensor location and setpoint were specified, the total airflow and pressure rise across the fan were used to iteratively solve for fan speed. This procedure was repeated for each hourly averaged system airflow condition to estimate fan energy. Additional duct size information, equipment specifications, fan performance data, and matrices are provided in Appendix A.

4.1 Use of Matrices to Convert Terminal Box Flows to Supply Duct Flows

The method outlined by Kalore et al. (2003) utilized matrix manipulation to calculate the amount of airflow throughout the system from individual terminal box airflows. This procedure relies on knowledge of the general connectivity of the terminal box branches and main supply duct.

The duct layout matrix is used to define the duct layout where *1* indicates a connection between a terminal box and a node and *0* the absence of any connection. The individual terminal box airflows are placed in the matrix of terminal box airflows. The transpose of the duct layout matrix multiplied by the matrix of terminal box airflows yields the matrix of supply duct node airflows. These airflows are passed to the model to calculate the losses throughout the system.

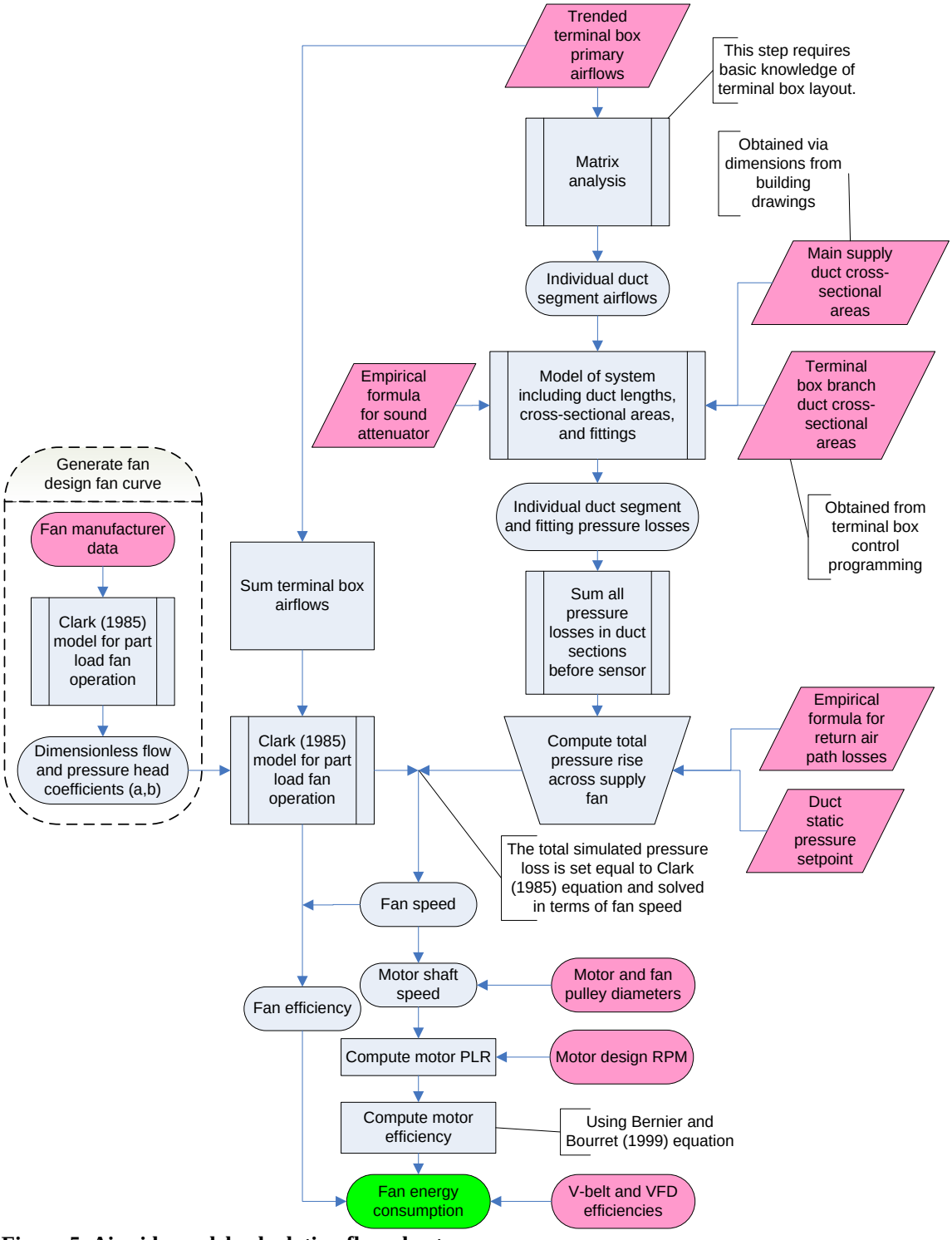

Figure 5. Air-side model calculation flow chart

$$\mathrm{L} = \begin{Bmatrix} & N_1 & N_2 & \ldots & \ldots & N_j \\ T_1 & 1 & 0 & \ldots & \ldots & 0 \\ T_2 & 0 & 0 & \ldots & \ldots & 1 \\ \ldots & \ldots & \ldots & \ldots & \ldots & \ldots \\ T_i & 1 & 1 & \ldots & \ldots & 0 \end{Bmatrix} \tag{4.1}$$

$$\mathrm{Q}_{\mathrm{term}} = \begin{Bmatrix} & \mathrm{Flow} \\ T_1 & \mathrm{cfm} \\ T_2 & \mathrm{cfm} \\ \ldots & \ldots \\ T_i & \mathrm{cfm} \end{Bmatrix} \tag{4.2}$$

$$\mathrm{Q}_{\mathrm{duct}} = \mathrm{L}^T Q_{\mathrm{term}} \tag{4.3}$$

where

L = duct layout matrix,

$\boldsymbol{Q}_{term}$ = matrix of terminal box airflows,

$\boldsymbol{Q}_{duct}$ = matrix of supply duct node airflows,

T_i = terminal box, and

N_j = node.

4.2 Calculating System Losses

The losses throughout the system were based on design duct and fitting information and the calculated supply duct airflows. The Reynolds number for each duct section was calculated assuming a constant specific gravity. This value was used to solve for the friction factor (Cengel and Turner 2005) and the corresponding pressure drop across each section of duct.

$$\mathrm{Re} = \frac{v \cdot D_h}{\upsilon} \tag{4.4}$$

$$\frac{1}{\sqrt{f}} \cong -1.8 \cdot \log\left[\frac{6.9}{\mathrm{Re}} + \left(\frac{\varepsilon / D_h}{3.7}\right)^{1.11}\right] \tag{4.5}$$

$$\Delta p_f = \frac{f \cdot L}{D_h}\left(\frac{v}{4005}\right)^2 \tag{4.6}$$

where

Re = Reynolds number,

υ = specific gravity (0.5525 ft^2/hr),

ε = absolute roughness of the duct (0.0003 ft) (ASHRAE 2005),

D_h = hydraulic diameter (ft),

f = friction factor,

L = length of duct (ft),

v = the air velocity (ft/min), and

Δp_f = frictional pressure drop (inWG).

The pressure loss due to fittings such as transitions, elbows, and tees were calculated based on the fitting loss coefficients tabulated in ASHRAE (2005).

$$\Delta p_{fitting} = C\left(\frac{v}{4005}\right)^2 \tag{4.7}$$

where

C = local loss coefficient,

$\Delta p_{fitting}$ = total pressure loss associated with particular fitting (inWG), and

v = the air velocity (ft/min).

In addition to the fittings listed above, it was found that AHU 5-1 was equipped with a sound attenuator. According to building design information, the attenuator created a pressure drop of 0.2 inWG at 7,500 CFM. Since the required field measurements to derive an empirical model were unobtainable, a quadratic relationship was developed based on the design information.

$$\Delta p_{atten} = 3.56 * 10^{-9} \cdot Q^2 \tag{4.8}$$

where

Q = total supply airflow (CFM) and

Δp_{atten} = total pressure drop across sound attenuator (inWG).

The velocity pressure at the static pressure sensor was calculated based on known duct dimensions and airflow. This value was added to the static pressure setpoint to obtain the total pressure at the sensor. The total pressure loss between the supply fan and the sensor was added to the total pressure at the duct sensor location to obtain the predicted total pressure leaving the supply fan.

The total pressure profile throughout the main supply ductwork was obtained by subtracting the individual duct losses from the predicted total pressure leaving the supply fan. The total pressure loss from each branch duct was subtracted from main supply duct pressure at the tee fitting to obtain the total pressure immediately upstream of each terminal box damper.

4.3 Modeling the Supply Air Fan

The fan blower design information was used to derive dimensionless flow, pressure head, and fan efficiency coefficients based on the method presented by Clark (1985). These coefficients were calculated for each design condition using the following equations:

$$\phi = \frac{\dot{m}}{\rho N d^3} \tag{4.9}$$

$$\psi = \frac{\Delta P_{sf}}{\rho N^2 d^2} \tag{4.10}$$

$$\eta_s = \frac{\dot{m} \Delta P_{sf}}{\rho \dot{W}_s} \tag{4.11}$$

where

Φ = dimensionless flow coefficient,

Ψ = dimensionless pressure head coefficient,

η_s = dimensionless fan efficiency coefficient,

$\dot{m}$ = mass flow rate,

N = fan rotational speed,

ρ = density,

ΔP_{sf} = fan static pressure rise across the fan,

$\dot{W}_s$ = power transmitted by the shaft, and

d = blower wheel diameter.

A fourth-order polynomial was fitted to the calculated data to obtain empirical flow and efficiency coefficients such that Equations 4.12 and 4.13 were satisfied. The coefficients for the supply fan at JEB AHU 5-1 are listed in Table 3.

$$\psi = a_o + a_1\phi + a_2\phi^2 + a_3\phi^3 + a_4\phi^4 \quad (4.12)$$

$$\eta_s = b_o + b_1\phi + b_2\phi^2 + b_3\phi^3 + b_4\phi^4 \quad (4.13)$$

where

a_n = empirical flow coefficient and

b_n = empirical efficiency coefficient.

Table 3. Dimensionless head and efficiency coefficients for experimental supply fan

Head	a_4	a_3	a_2	a_1	a_0
	3.130281	-14.1449	20.02799	-13.2786	8.121875
Efficiency	b_4	b_3	b_2	b_1	b_0
	-0.10394	-0.1588	0.224465	0.294922	0.52804

4.4 Predicting Fan Energy Consumption

During the afternoon of March 12, 2009 the fan speed and duct static pressure setpoint were temporarily fixed at their existing values to enable the measurement of static pressure and total supply airflow. Due to the abrupt change in duct direction at the fan discharge and the

spatial constraints in the mechanical room, the total supply airflow was obtained indirectly through measurements of the return and outside airflows. The static pressure measured between the cooling coil and supply fan inlet was -0.23 inWG and the total supply airflow was 3,275 CFM. The result was an empirically derived equation for fan inlet static pressure as a function of airflow, which was used to compute the total pressure at the fan inlet.

$$P_{s1} = -2.14439 * 10^{-8} \cdot Q^2 \tag{4.14}$$

$$P_{v1} = \left(\frac{Q / A_{c1}}{4005} \right)^2 \tag{4.15}$$

$$P_{t1} = P_{s1} + P_{v1} \tag{4.16}$$

where

Q = total supply airflow (CFM),

A_{c1} = cross-sectional area of the cooling coil (16.7 ft^2),

P_{t1} = total pressure at the fan inlet (inWG),

P_{s1} = static pressure at fan inlet (inWG), and

P_{v1} = velocity pressure at the fan inlet (inWG).

The total pressure at the fan inlet was used to calculate the static pressure rise across the fan using the previously calculated total pressure at the fan discharge.

$$P_{v2} = \left(\frac{Q / A_{c2}}{4005} \right)^2 \tag{4.17}$$

$$P_{sf} = \left(P_{t2} - P_{t1}\right) - P_{v2} \tag{4.18}$$

where

Q = total supply airflow (CFM),

P_{sf} = static pressure rise across fan (inWG),

P_{v2} = velocity pressure at the fan discharge (inWG),

A_{c2} = cross-sectional area of the supply fan discharge (3.45 ft^2),

P_{t1} = total pressure at the fan inlet (inWG), and

P_{t2} = total pressure at the fan discharge (inWG).

The dimensionless equations by Clark (1985) were used to derive the following expression to iteratively solve for the fan speed that would yield the predicted static pressure rise across the fan. The mass flow rate in this equation was calculated using the sum of the terminal box primary airflows.

$$\frac{P_{sf}}{\rho N^2 d^2} = a_o + a_1\left(\frac{\dot{m}}{\rho N d^3}\right) + a_2\left(\frac{\dot{m}}{\rho N d^3}\right)^2 + a_3\left(\frac{\dot{m}}{\rho N d^3}\right)^3 + a_4\left(\frac{\dot{m}}{\rho N d^3}\right)^4 \qquad (4.19)$$

This fan speed was used to solve for shaft efficiency and motor shaft speed using a ratio of field measured pulley speeds. The measured fan and motor pulley speeds were 1060 and 836 RPM respectively. The supporting documentation for the tachometer as well as the instrumentation used to measure airflow and static pressure is provided in Appendix B.

V-belts have a peak efficiency ranging from 93 to 98% at the time of installation; however, if they are not periodically re-tensioned increased slippage can result in a 5% reduction (U.S. Department of Energy 2005). Older VFDs disturbed the sine wave and caused reduced drive and motor efficiencies; however, modern VFDs do not have this effect and have efficiencies ranging from 95 to 98%. For most applications of 10 HP and above, an efficiency of 97%[1] may be assumed (Rishel 2003).

The motor efficiency was calculated as a function of part load ratio (PLR) using the equation presented by Bernier and Bourret (1999). Although this equation was originally intended for motors exceeding 20 HP, its superposition onto the 10 HP high efficiency motor curve presented by Natural Resources Canada (2004) shown in Figure 6 justified its use in the model.

[1] The installed VFD efficiency documented by manufacturer was also 97% (Danfoss Inc. 2005).

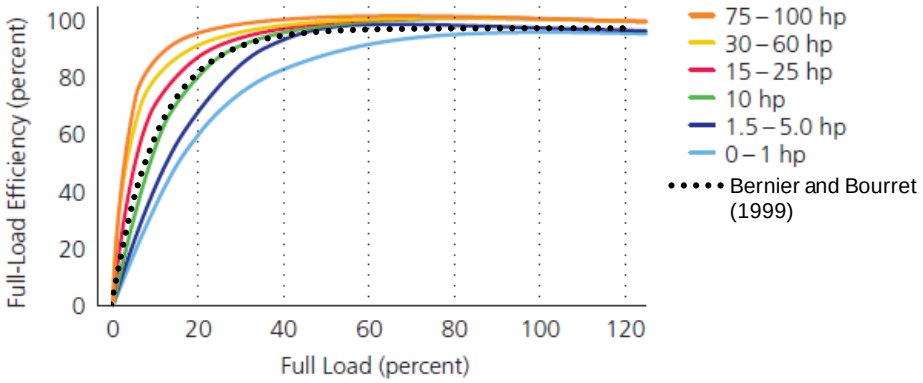

Figure 6. Representative motor efficiency curves for various HP ranges (Natural Resources Canada 2004)

$$\eta_{motor} = 94.187(1 - e^{-0.0904 \cdot PLR}) \tag{4.20}$$

$$\dot{W}_{theo} = \frac{\dot{m}\Delta P_{sf}}{\rho} \tag{4.21}$$

$$\dot{W}_{in} = \frac{\dot{W}_{theo}}{\eta_s \eta_{belt} \eta_{motor} \eta_{VFD}} \tag{4.22}$$

where

$\dot{m}$ = mass flow rate,

PLR = fraction of design motor speed,

ρ = density,

ΔP_{sf} = fan static pressure rise across the fan,

$\dot{W}_s$ = power transmitted by the shaft,

W_{theo} = theoretical fan power,

W_{in} = total input power,

η_s = dimensionless fan efficiency coefficient,

η_{belt} = v-belt efficiency (0.93),

η_{VFD} = VFD efficiency (0.97), and

η_{motor} = motor efficiency.

4.5 Model Simplifications

- The fitting loss coefficients provided by ASHRAE (2005) do not account for the additional pressure loss associated with closely coupled fittings. This extra pressure loss was neglected in the model.
- All of the flexible branch ductwork was assumed to be fully extended.
- The minimum pressure required at the inlet to each terminal box to ensure proper operation was neglected.
- The pressure loss associated with the duct and diffusers downstream of each terminal box was neglected.
- All of the splits that appear in the building design drawings were simulated as wyes.
- The pressure drop across the filters was assumed to only be a function of airflow. Increased pressure drop across the filters associated with time and the accumulation of particulates was neglected.
- The supply air temperature was assumed constant throughout the ductwork.
- The slightly positive pressure in the conditioned space was neglected and a neutral pressure was assumed.
- The model does not directly simulate duct leakage or individual component controllers.

4.6 Model Calibration

A test to verify the static pressure sensor was performed on March 17, 2009. The static pressure was measured at the location of the duct sensor while varying the setpoint from 0.5 to 2.0 inWG in APOGEE using 0.25 inWG increments. After sufficient time was given to allow the system to adjust, the duct static pressure was recorded. The resulting slope and intercept

shown in Equation 4.23 were used in the model to adjust the trended duct static pressure measurements.

$$P_{field} = 0.7514 \cdot P_{EMCS} - 0.2664 \tag{4.23}$$

where

P_{field} = field measured duct static pressure at sensor (inWG) and

P_{EMCS} = trended duct static pressure (inWG).

During the afternoon of March 12, 2009 a field test was performed. Since the control programming had been modified to include demand based SPR control, the existing fan speed was fixed and sufficient time was given to allow the system to adjust prior to taking the measurements. In addition, the observed system change resulting in higher VFD speeds had already occurred; therefore, only the airflow measurement was used to calibrate the model. The field measured values and trend data from the same day and time period (15:45) are provided in Table 4.

Table 4. Summary of AHU field measurements taken on March 12, 2009

Parameter	Field measurements	Trend data
AHU supply airflow (CFM)	3,275	2,776
Blower speed (RPM)	1,060	N/A
Motor speed (RPM)	836	836
Fan total pressure rise (inWG)	0.92	N/A

A comparison of the measured and trended AHU supply airflow values revealed a discrepancy of approximately 400 CFM. No further work was performed to investigate this difference; however, possible explanations include out of calibration terminal box airflow sensors and duct leakage. The trend data was modified by applying a factor of 1.18 to the terminal box supply airflows and the empirical slope and intercept values to the duct static

pressures to obtain the results shown in Figure 7. In addition, the results in Table 5 verify that trended VFD speed is an accurate representation of motor shaft speed.

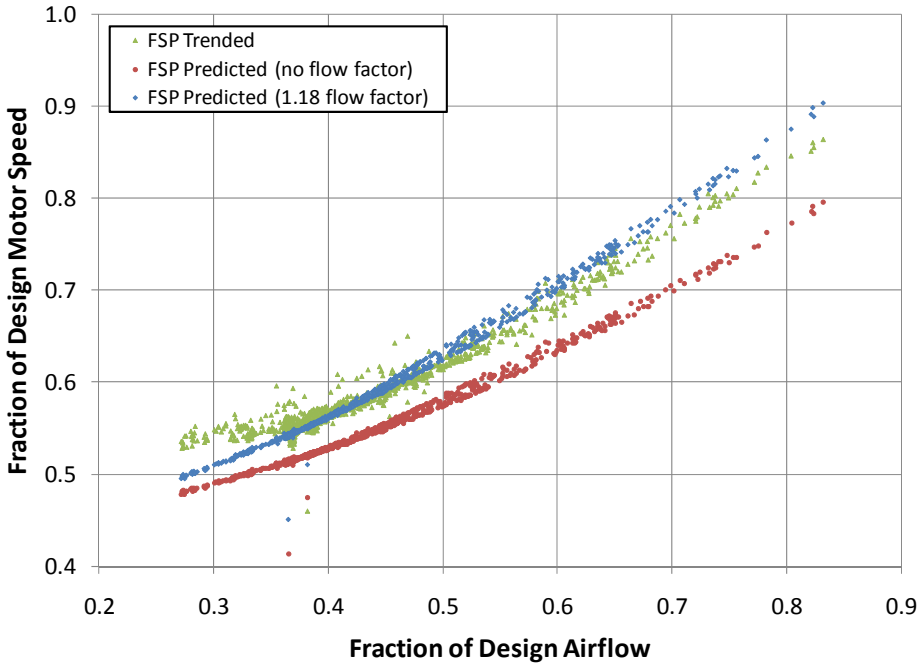

Figure 7. Model calibration results during FSP control using airflow trend data from November 1, 2008 to February 12, 2009

Table 5. Field verification of VFD and motor performance

Field values	Calculated values
VFD display: 28.3 Hz Measured motor shaft speed: 836 RPM Design motor speed: 1760 RPM	$RPM = RPM_{des}\left(\frac{VFD}{VFD_{des}}\right)$ $RPM = 1760\left(\frac{28.3}{60}\right) = 839$

This calibration process was driven by measurements of total supply airflow and duct static pressure. The intent of this model was not to precisely duplicate the experimental system, but to verify that its output was consistent with a typical system.

5. PROJECT RESULTS

This chapter presents the simulated power required to supply the trended airflow data from November 1, 2008 to February 12, 2009 through the system model using various static pressure control methods. In addition to FSP control, the model was used to simulate SPR control based on zonal demand, system demand, and outside air temperature.

5.1 Investigation of Zonal Demand Based SPR Control

The concept of model predicted control (Ahmed 2001; Cascia 2007; Goswami 1986; Kalore et al. 2003; Okada et al. 1992) was added to the model to derive an optimized static pressure setpoint (OptSPR) for each set of hourly averaged terminal box airflows. This setpoint represents the maximum terminal box total pressure requirement, which in turn is used to establish the minimum static pressure setpoint at the sensor located near the discharge of the fan.

$$P_{req,i} = P_{duct} + P_{flow} \tag{5.1}$$

$$P_{opt,total} = \max\left(P_{req,i}\right) \tag{5.2}$$

$$P_{opt,SPR} = P_{opt,total} - P_{v,sensor} \tag{5.3}$$

where

$P_{req,i}$ = total pressure required to supply flow to each zone *i* (inWG),

P_{duct} = total pressure loss associated with supply duct (inWG),

P_{flow} = total pressure required to provide airflow at the terminal box (inWG),

$P_{opt,total}$ = optimized total pressure requirement at the sensor (inWG),

$P_{v,sensor}$ = velocity pressure measured at the sensor (inWG), and

$P_{opt,SPR}$ = optimized static pressure requirement at the sensor (inWG).

5.1.1 Validation of Simulated Zonal Demand Based SPR Control

Given the change in system performance documented in Chapter 3 (Section 4), the model was re-calibrated using field measurements and trend data. The steps taken to calibrate

the baseline model, which are summarized in Table 6, were intended to systematically increase the overall resistance of the system. Due to the issues associated with 15 minute data trended during SPR control, COV trend data from April 21, 2009 was used to validate the use of OptSPR as a way to simulate the SPR control strategy implemented at JEB. The motor speeds predicted by the re-calibrated model under OptSPR control, using the COV trended airflows, is compared with the COV trended VFD speeds in Figure 8.

Table 6. Model calibration steps during SPR control using field measured data

Parameter	Baseline	Factor of 1.18 to airflows	Factor of 4 to duct lengths	Factor of 2 to fitting loss coefficients	Field measured
AHU supply airflow (CFM)	2,776	3,276	3,276	3,276	3,275
Blower speed (RPM)	896	986	1,008	1,030	1,060
Motor speed (RPM)	707	778	795	812	836
Fan total pressure rise (inWG)	0.79	0.90	0.96	1.02	0.92

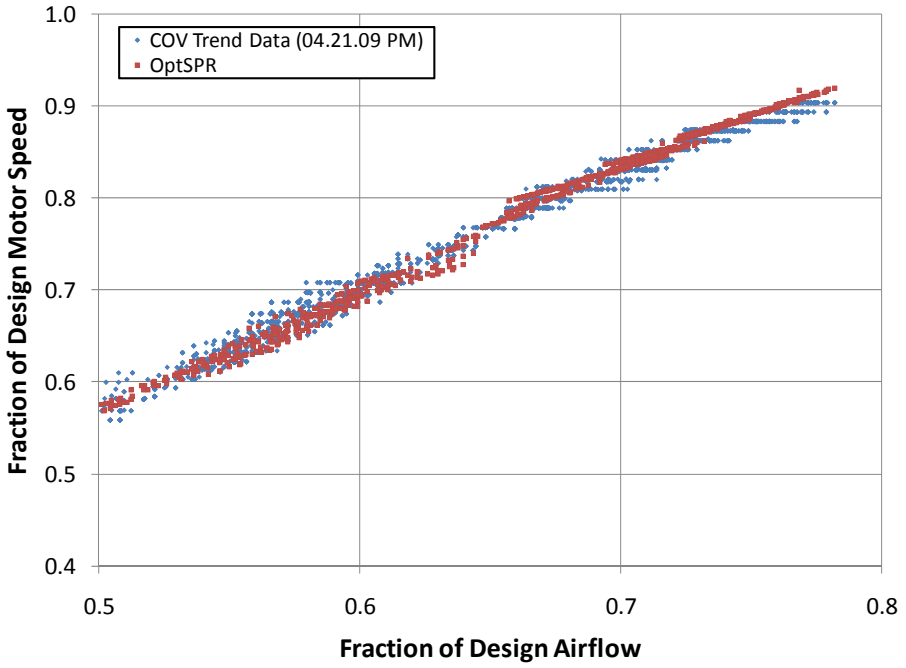

Figure 8. Fraction of design motor speed required during JEB SPR control and simulated OptSRP control using COV trend data from the afternoon of April 21, 2009

5.1.2 Baseline Performance

The simulated fraction of design motor speed required during FSP and OptSPR control using the trended airflow data from November 1, 2008 to February 12, 2009 is shown in Figure 9. The amount of scatter shown during OptSPR control is due to the range of static pressure setpoints selected for identical system airflow ratios.

A closer evaluation of the simulated OptSPR power requirements revealed that terminal boxes FVV 5-1 and FVV 5-4 consistently had the highest pressure requirements. The terminal box control setpoints for FVV 5-4 indicated that the design maximum cooling airflow setpoint had been overridden. In addition, a field investigation found that the thermostat corresponding to FVV 5-1 was being influenced by a nearby computer. In order to simulate the system as it was originally designed, the trended airflow data corresponding to these terminal boxes was

modified using the procedure documented in Appendix C. These modified airflows would be used to simulate system performance for each method of duct static pressure control.

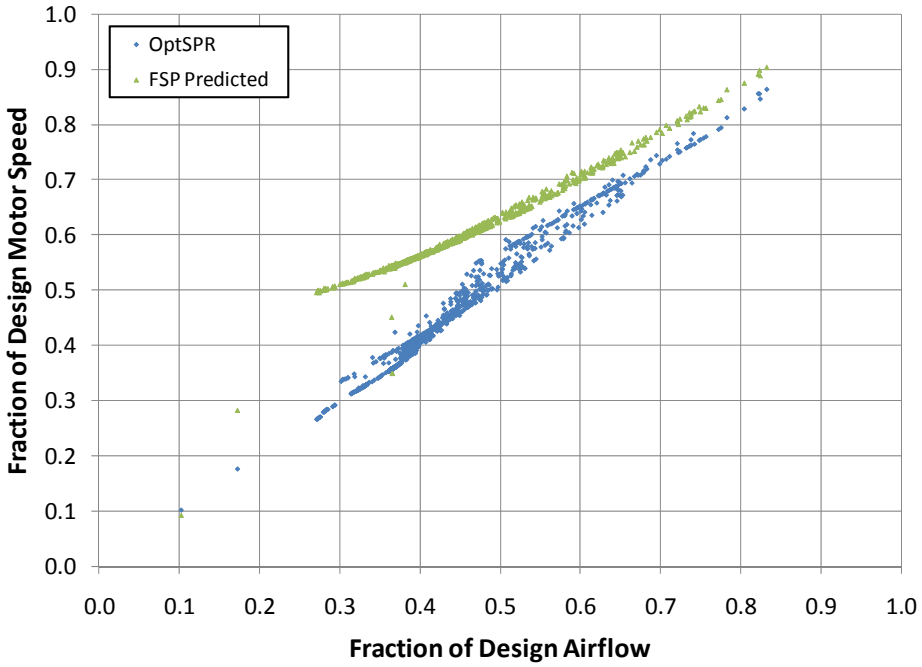

Figure 9. Fraction of design motor speed required to supply the same airflow during simulated FSP and OptSPR control using hourly averaged 15 minute trended airflow data from November to February

The zonal demand based SPR control baseline performance shown in Figure 10 illustrates the combined effect of the modified terminal box airflows. The power requirement under these conditions was found to be 116% of that required by the ideal reset. The remaining scatter is due to the non-simultaneous loads in the zones served by the experimental AHU. It was also observed that while one terminal box had the highest pressure requirement at a given system airflow ratio, the static pressure setpoint (and power required) increased with zone load ratio (Appendix C).

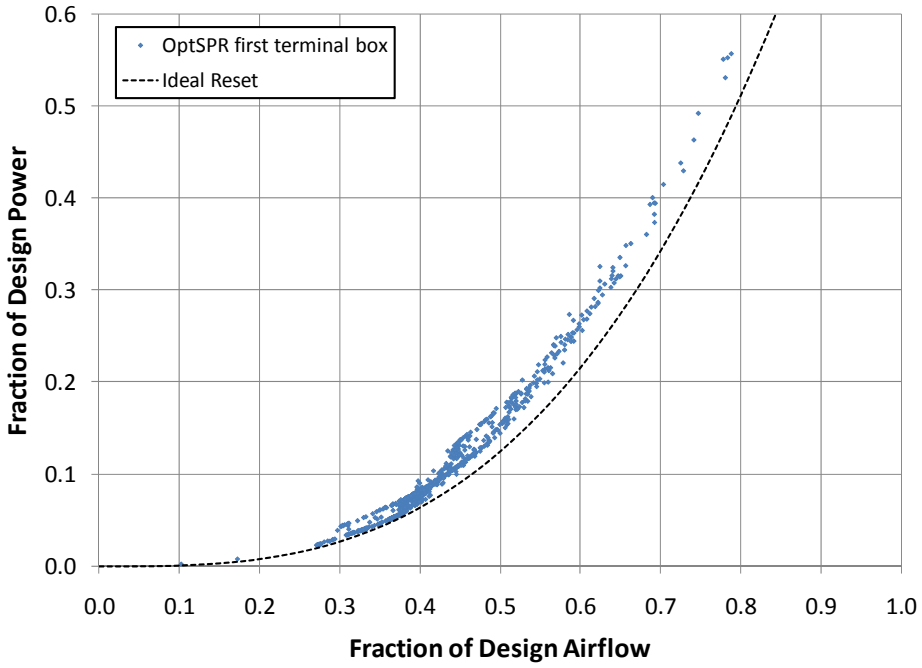

Figure 10. Fraction of design power required during OptSPR control using adjusted hourly averaged 15 minute trend airflow data from November to February

5.1.3 Impact of Reset Criteria on Overall Performance

The baseline zonal demand based SPR control was modified such that the OptSPR setpoint was based on the terminal box with the second highest pressure requirement. The results shown in Figure 11 indicate that neglecting the terminal box with the highest pressure requirement leads to a closer approximation of the ideal reset curve. The power requirement under these conditions was found to be 109% of that required by the ideal reset. The further reduction in scatter would indicate that for many of the simulated hours one zone has a significantly higher load ratio than the others. During these periods it was observed that a considerable portion of the OptSPR setpoint is to overcome the friction in the branch duct at the maximum terminal box airflow setpoint.

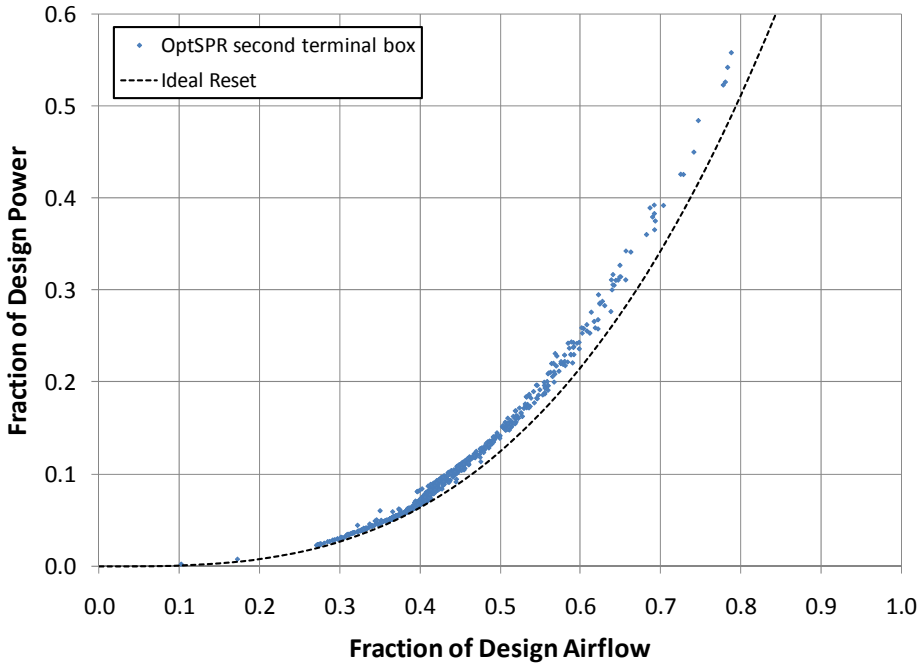

Figure 11. Fraction of design power required during OptSPR control using adjusted hourly averaged 15 minute trend airflow data from November to February based on the second most critical zone

5.2 Investigation of System Demand Based SPR Control

The baseline control was converted to a system demand based SPR control using the equations developed by Liu and Liu (2008). This method expands upon the quadratic relationship between pressure and airflow by incorporating a load factor. This factor is an indication of the system load distribution and can vary from 15%, when the zones have similar load ratios, up to 30% when the zone load ratios are diverse. The load factor was varied from 15 to 30% and the minimum and maximum static pressure setpoints were set to the field measured values.

$$p_{set} = \max\left(\left(p_{set,\max} - p_{ref}\right)\left(\frac{Q}{Q_d}\right)^2 + p_{ref}, p_{\min} \right) \tag{5.4}$$

$$p_{ref} = LF \cdot p_{set,\max} \tag{5.5}$$

where

p_{set} = static pressure setpoint (inWG),

$p_{set,max}$ = maximum static pressure setpoint (inWG),

p_{min} = maximum static pressure setpoint (inWG),

p_{ref} = reference static pressure (inWG),

LF = load factor,

Q = supply airflow (CFM), and

Q_d = design supply airflow (CFM).

The simulated results are shown for a 30% load factor with the sensor positioned ~2/3 down the supply duct in Figure 12 and near the fan discharge in Figure 13. The same procedure was used to obtain curves with a 15% load factor. In both cases, moving the sensor to a position near the fan discharge reduced the required motor speeds and the amount of data scatter (Figure 14).

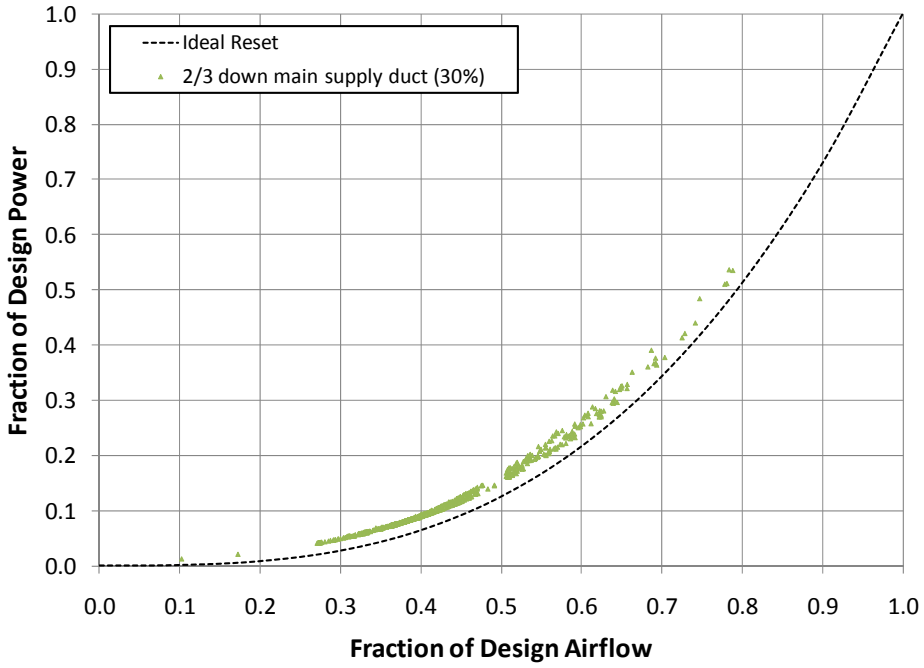

Figure 12. Fraction of design power required during airflow based SPR control using adjusted hourly averaged 15 minute trend airflow data from November to February, a 30% load factor, and sensor position approximately 2/3 down the duct

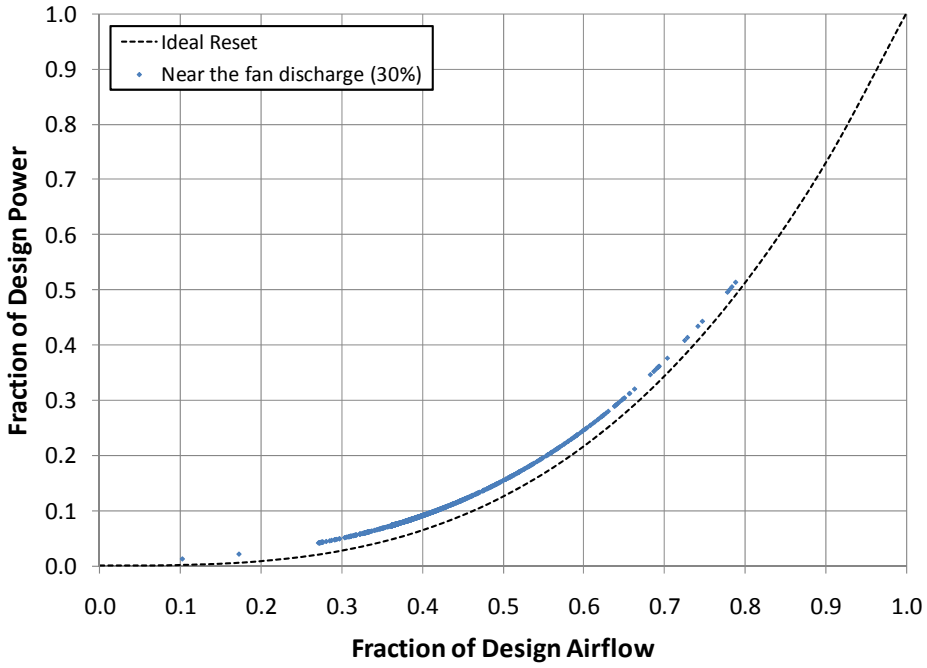

Figure 13. Fraction of design power required during airflow based SPR control using adjusted hourly averaged 15 minute trend airflow data from November to February, a 30% load factor, and sensor position near the fan discharge

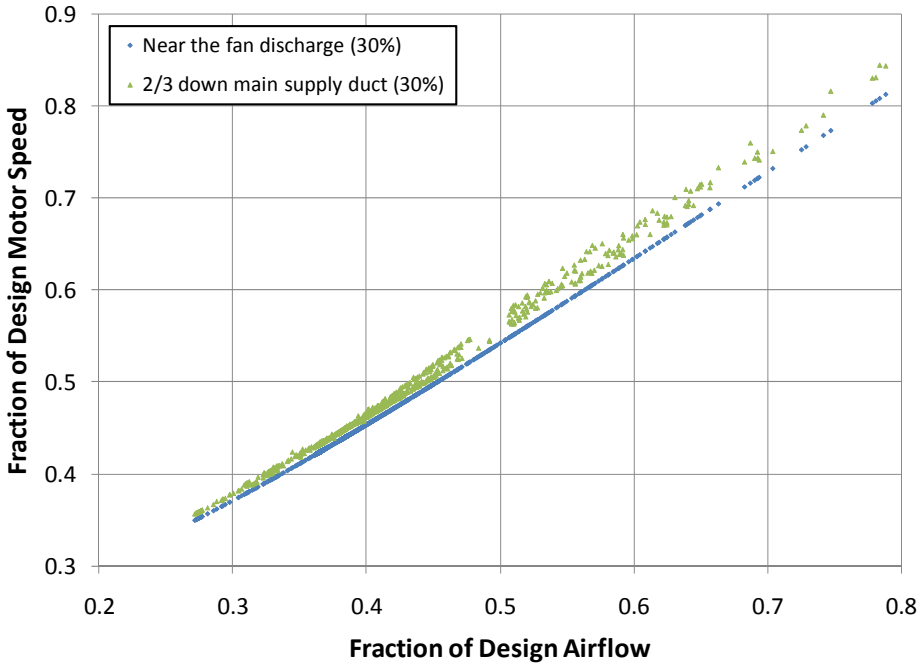

Figure 14. Fraction of design motor speed required during airflow based SPR control using adjusted hourly averaged 15 minute trend airflow data from November to February, a 30% load factor, and varying the sensor position

5.3 Investigation of Outside Air Temperature Based SPR Control

The baseline control was converted to an outside air temperature (OAT) based SPR control using the actual sensor position (~2/3 down supply duct) and the field measured minimum and maximum static pressure setpoints. The hourly averaged outside air temperatures for Easterwood Airport in College Station, Texas were obtained from NCDC (2009). The result of linearly resetting the setpoint according to the temperature range 50 to 90°F is shown in Figure 15. The energy required under this control was 122% of that required by the ideal reset. Points lying below the ideal curve represent times when the duct static pressure was not high enough to supply the required terminal box airflows.

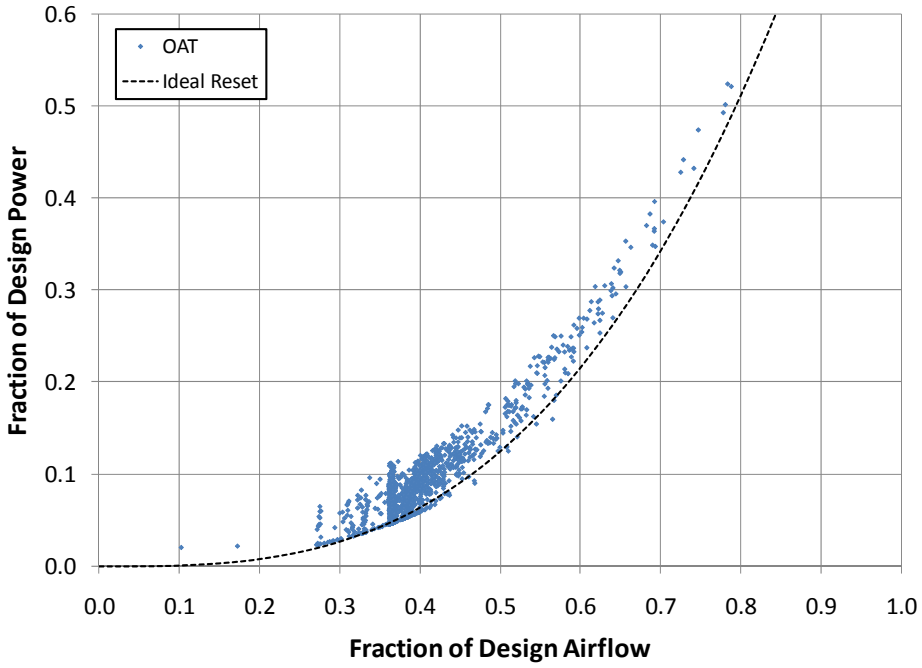

Figure 15. Fraction of design power required during outside air temperature based SPR control using adjusted hourly averaged 15 minute trend airflow data from November to February

5.4 Investigation of FSP Control

In a system with FSP control the recommended static pressure sensor location is 75 to 100% of the distance from the first to the most remote terminal box (ASHRAE 2007b). Since the experimental AHU at JEB falls under this recommendation, the model was used to estimate the power required to maintain FSP setpoints of 1, 2, and 3 inWG. Figure 16 illustrates the hourly power requirements for a FSP setpoint of 2 inWG.

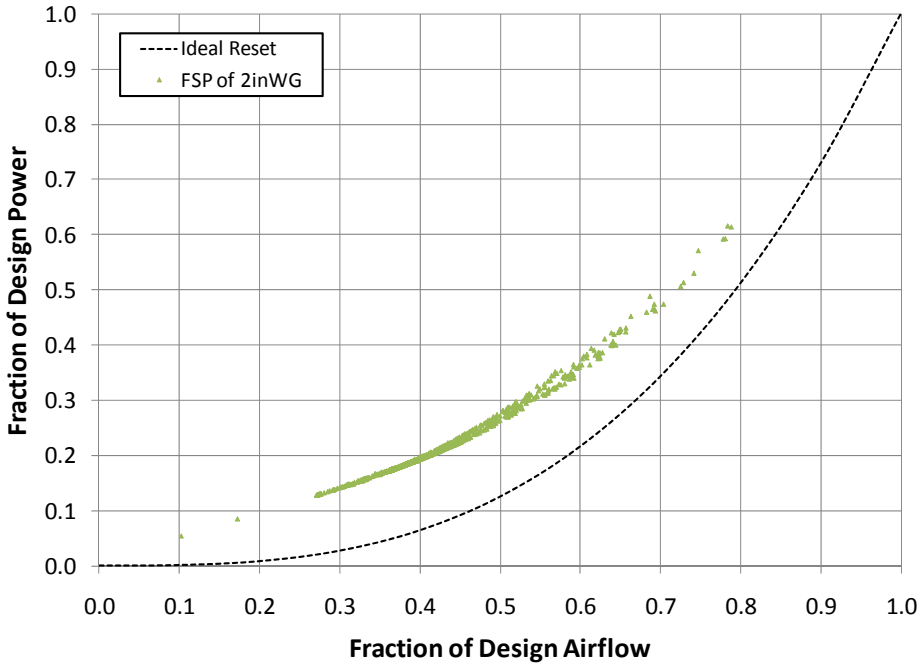

Figure 16. Fraction of design power required during FSP control using adjusted hourly averaged 15 minute trend airflow data from November to February and a setpoint of 2 inWG

5.5 Analysis of Simulation Results

A summary of the simulated static pressure control strategies is provided in Table 7. For each hour from November 1, 2008 to February 12, 2009, the difference in total fan energy was computed assuming a FSP setpoint of 2 inWG as the baseline form of control. The sum of this difference expressed as a fraction of the total fan energy corresponding to the baseline control yielded the savings.

Table 7. Estimated fan energy savings assuming a baseline FSP setpoint of 2 inWG

Static Pressure Control	Sensor location	Details	Savings
Demand1	Fan discharge	Based on 1st damper	73%
Demand2	Fan discharge	Based on 2nd damper	74%
OAT	Typical (~2/3)	Linear between 50 and 90°F	65%
FSP3	Typical (~2/3)	Static pressure fixed at 3 inWG	-45%
FSP1	Typical (~2/3)	Static pressure fixed at 1 inWG	41%
AFdis30	Fan discharge	Load ratio of 30%	62%
AFdis15	Fan discharge	Load ratio of 15%	67%
AFtyp30	Typical (~2/3)	Load ratio of 30%	59%
AFtyp15	Typical (~2/3)	Load ratio of 15%	64%

The highest savings (73-74%) were achieved using zonal demand based SPR control. System demand based SPR control yielded savings ranging from 59 to 76%, which increased when the duct sensor was positioned near the fan discharge and under similar zone load conditions. The outside air temperature based SPR control yielded savings of 65% since the experimental system supplied primarily perimeter zones. Finally, increasing the FSP setpoint from 2 to 3 inWG increased fan energy by 45%, while decreasing the setpoint from 2 to 1 inWG decreased fan energy by 41%.

6. SUMMARY AND RECOMMENDATIONS

6.1 Summary

The existing literature pertaining to SPR control has been organized into a flow chart tool to facilitate the selection of a strategy based on system requirements. This process was used to identify three major categories of SPR control: zonal demand based, system demand based, and use of indirect measurements often related to building load. For situations where multiple strategies apply to a particular system, this tool does not yet have the ability to recommend the optimal method.

A calibrated model was developed based on building design information for a typical single duct VAV system (non-loop) with an airfoil type supply fan and a fixed discharge air temperature. The model was constrained by the field measured minimum and maximum static pressure setpoints and includes the effect of the fan, v-belt, motor, and VFD. This model was used to simulate a representative SPR control strategy from each category as well as FSP control. While utilizing trend data from November 1, 2008 to February 12, 2009, the FSP control of the experimental system was used as the baseline for ranking the energy savings potential of nine different forms of duct static pressure control.

The highest savings (73-74%) were achieved using zonal demand based SPR control. System demand based SPR control yielded savings ranging from 59 to 76%, which increased when the duct sensor was positioned near the fan discharge and under similar zone load conditions. The outside air temperature based SPR control yielded savings of 65% since the experimental system supplied primarily perimeter zones. Finally, increasing the FSP setpoint from 2 to 3 inWG increased fan energy by 45%, while decreasing the setpoint from 2 to 1 inWG decreased fan energy by 41%.

In addition, the simulated motor speeds associated with model predicted control were found to agree with the trended data during SPR control based on terminal box damper position. This confirms that sensor location is less critical for zonal demand based SPR control when compared to FSP control; however, when system demand based (e.g. total airflow) SPR control was implemented an energy penalty was observed when the sensor was located down the supply duct as opposed to near the fan discharge.

6.2 Recommendations

A shortcoming of the SPR strategy selection flow chart tool arises when multiple strategies apply to a particular system. Future work may address this limitation by identifying additional system characteristics that will enable the tool to recommend the most energy efficient SPR control strategy.

The creation of this model and the collection of building performance data enable several possibilities for future study. The following elements of the model may be addressed by future researchers:

- The airfoil type supply air fan: The current dimensionless fan performance coefficients derived using the procedure by Clark (1985) may be updated using alternative performance data.
- AHU supply air temperature: The trended terminal box data (primary airflow and reheat valve position) may be used analyze the effect of simultaneously resetting the duct static pressure and discharge air temperature setpoints.
- Return air fan and terminal box pressure requirements: These elements may be added to the model to examine their impact on simulated supply fan energy.

- Minimum and maximum static pressure setpoints: These values are currently based on field measured values for the experimental system; however, other representative values could be simulated.
- Existing ductwork: The model was based on the installed non-loop ductwork found in the experimental building. The series of matrix operations used to solve for the airflow through the system may be modified to assume a loop configuration (Kalore et al. 2003).
- Supply fan power: The model estimated supply fan power using fan performance data, trended airflows, and efficiency assumptions. It is recommended that an additional control point for the output VFD power be added to the EMCS and trended to further validate the model.

REFERENCES

Ahmed, O. 2001. A model based control for variable volume distribution system. *Proceedings of Clima2000 World Congress, Naples, Italy*. Available on CDROM.

ASHRAE. 2005. *2005 ASHRAE Handbook – Fundamentals*. Atlanta: American Society of Heating, Refrigerating and Air-Conditioning Engineers, Inc.

ASHRAE. 2007a. *ANSI/ASHRAE/IESNA Standard 90.1-2007, Energy Standard for Buildings Except Low-Rise Residential Buildings.* Atlanta: American Society of Heating, Refrigerating and Air-Conditioning Engineers, Inc.

ASHRAE. 2007b. 2007 *ASHRAE Handbook – HVAC Applications*. Atlanta: American Society of Heating, Refrigerating and Air-Conditioning Engineers, Inc.

Bernier, M., and B. Bourret. 1999. Pumping energy and variable frequency drives. *ASHRAE Journal* 41(12):37-40.

Brightbill, E.L., and J.P. Rutt. 1998. Using EMCS data to document and improve air handler performance. *Proceedings of the 11th Annual Symposium on Improving Building Energy Efficiency in Hot and Humid Climates, Ft. Worth, TX.* http://esl.eslwin.tamu.edu/digital-library.html.

Cascia, M. 2007. A method of optimizing VAV fan static pressure setpoint using model-based control. ASHRAE Winter Meeting, January 27-31. Dallas, TX. Available on CDROM.

CCC. 2008. Fan System Workbook, Version 2.0. California Commissioning Collaborative, Sacramento, CA. http://www.cacx.org/resources/rcxtools/spreadsheet_tools.html.

Cengel, A.Y., and R.H. Turner. 2005. *Fundamentals of Thermal-Fluid Sciences*. New York: McGraw-Hill.

Chicago Blower Corporation. 2006. Design 51: Double width airfoil fans. Report DFO-102, Chicago Blower Corporation, Glendale Heights, IL. www.chiblo.com/bulletins/DFO-102.pdf.

Clark, D.R. 1985. HVACSIM+ building systems and equipment simulation program reference manual. Report NBSIR 84-2996, U.S. Department of Commerce, National Bureau of Standards, National Engineering Laboratory, Center for Building Technology, Building Equipment Division, Gaithersburg, MD.

Danfoss Inc. 2005. VLT® 6000 series drives for HVAC. Report 175R5326, Danfoss HVAC/R, Milwaukee, WI. www.danfoss.com/North_America/BusinessAreas/DrivesSolutions/Literature.htm.

Dong, D., M. Liu, and J. Wang. 2005. Continuous Commissioning® of a single fan dual duct system in an office building, *Proceedings of the* 5th *International Conference for Enhanced Building Operations, Pittsburgh, PA*. http://esl.eslwin.tamu.edu/digital-library.html.

EIA. 2006. 2003 commercial buildings energy consumption survey (CBECS), detailed tables, October 2006. Energy Information Administration, U.S. Department of Energy, Washington, DC. http://www.eia.doe.gov/emeu/cbecs.

Englander, S.L., and L.K. Norford. 1992. Saving fan energy in VAV systems – Part 2: Supply fan control for static pressure minimization using DDC zone feedback. *ASHRAE Transactions* (98)1:19-32.

EPA. 2008. QuikFan, Version 4.0. Energy Star Buildings, U.S. Environmental Protection Agency, Atmospheric Pollution Prevention Division, Washington, DC. http://www.cleanaircounts.org/moreenergystarbuildings.aspx.

Evans, C., J. Cordero, M. Atencio, D.E. Claridge, J. Martinez, C. Oberle, J.C. Baltazar-Cervantes, and Y. Zhu. 2005. Continuous Commissioning® of an office/laboratory building. *Proceedings of the 5th International Conference for Enhanced Building Operations, Pittsburgh, PA*. http://esl.eslwin.tamu.edu/digital-library.html.

Federspiel, C.C. 2003. Energy-efficient air-handling controls feasibility analysis. Report P500-03-052F, California Energy Commission, Sacramento, CA. http://www.energy.ca.gov/research/innovations/eisg_final_reports/500-03-052/500-03-052.PDF.

Federspiel, C.C. 2005. Detecting critical supply duct pressure. *ASHRAE Transactions* 111(1):957-63.

Goswami, D. 1986. VAV fan static pressure control with DDC. *Heating/Piping/Air Conditioning Engineering: HPAC* 58(12):113-117.

Haasl, T., A. Potter, L. Irvine, and L. Luskay. 2001. Retrocommissioning's greatest hits. *Proceedings of the 1st International Conference for Enhanced Building Operations, Austin, TX.* http://esl.eslwin.tamu.edu/digital-library.html.

Hartman, T. 1989. TRAV - A new HVAC concept. *Heating/Piping/Air Conditioning Engineering: HPAC* 61(7):69-73.

Hartman, T. 1993. Terminal regulated air volume (TRAV) systems. *ASHRAE Transactions* 99(1):791-800.

Hartman, T. 1995. Global optimization strategies for high-performance controls. *ASHRAE Transactions* 101(2):679-87.

Hydeman, M., and J. Stein. 2003. A fresh look at fans. *Heating/Piping/Air Conditioning Engineering: HPAC* 75(5):28-41.

Kalore, P., A. Osman, and M. Cascia. 2003. Dynamic control of a building fluid distribution system. *Proceedings of the IEEE Conference on Control Applications, Istanbul, Turkey,* pp. 2:1215-20.

Khoo, I., G.J. Levermore, and K.M. Letherman. 1997. Duct loops and VAV modeling and control. *Proceedings of Clima2000 World Congress, Brussels, Belgium*. Available on CDROM.

Lee, R.L.Y., and T. Chow. 2004. Performance of variable-air-volume air-conditioning system under reduced static pressure control in an occupied office. *Architectural Science Review* 47(1):63-70.

Levermore, G.J. 2005. Duct loop systems - Savings and performance. *ASHRAE Transactions* 111(1):507-14.

Liu, C., S. Deng, D.E. Claridge, and W.D. Turner. 2000. Lessons learned from the continuous commissioning of a multi-functional commercial building. *Proceedings of the 12th Annual Symposium on Improving Building Energy Efficiency in Hot and Humid Climates, San Antonio, TX.* http://esl.eslwin.tamu.edu/digital-library.html.

Liu, G., and M. Liu. 2008. Supply fan control methods for VAV systems using a fan airflow station. *ASHRAE Transactions* 114(2):451-57.

Liu, M., M. Abbas, B. Veteto, D.E. Claridge, and H. Bruner. 1998. Impacts of optimized cold & hot deck reset schedules on dual duct VAV system – Application and results. *Proceedings of the 11th Annual Symposium on Improving Building Energy Efficiency in Hot and Humid Climates, Ft. Worth, TX*. http://esl.eslwin.tamu.edu/digital-library.html.

Liu, M. 2002. Variable speed drive volumetric tracking (VSDVT) for airflow control in variable air volume (VAV) systems. *Proceedings of the 13th Annual Symposium on Improving Building Energy Efficiency in Hot and Humid Climates, Houston, TX.* http://esl.eslwin.tamu.edu/digital-library.html.

Liu, M., D.E. Claridge, and W.D. Turner. 2002. Continuous Commissioning[SM] guidebook for federal energy managers. Federal Energy Management Program, U.S. Department of Energy, Washington, DC. www1.eere.energy.gov/femp/operations_maintenance/om_ccguide.html.

Liu, M., J. Feng, Z. Wang, L. Wu, K. Zheng, and X. Pang. 2007a. Impacts of static pressure reset on VAV system air leakage, fan power and thermal energy – Part 1: Theoretical model and simulation. *Proceedings of the 7th International Conference for Enhanced Building Operations, San Francisco, CA*. http://esl.eslwin.tamu.edu/digital-library.html.

Liu, M., K. Zheng, L. Wu, Z. Wang, and C. Johnson. 2007b. Impacts of static pressure reset on VAV system air leakage, fan power and thermal energy – Part 2: Case demonstration for a typical climate system. *Proceedings of the 7th International Conference for Enhanced Building Operations, San Francisco, CA*. http://esl.eslwin.tamu.edu/digital-library.html.

Lorenzetti, D.M., and L.K. Norford. 1993. Pressure reset control of variable air volume ventilation systems. *Proceedings of the ASME International Solar Energy Conference, Washington, DC,* 445-53.

Martinez, J.T., W.D. Turner, and J.C. Baltazar. 2007. Continuous Commissioning® of the Reynolds army community hospital: Fort Sill, Oklahoma. *Proceedings of the 7th International Conference for Enhanced Building Operations, San Francisco, CA*. http://esl.eslwin.tamu.edu/digital-library.html.

Mikec, P. Wolf Equipment Sales. Email from author, March 13, 2009.

Monarch Instrument. 2009. Pocket-tach plus kit, instruction manual. Report 1071-4835-001, Monarch Instrument, Amherst, NH. http://www.monarchinstrument.com/pdfs/manuals/1071-4835-001%20PT+%20Eng.pdf.

Napper, G., G. Wei, D. Turner, J.C. Baltazar-Cervantes, D. Dong, L. Song, and I.S. Joo. 2007. Continuous Commissioning® of public schools. *Proceedings of the 7th International Conference for Enhanced Building Operations, San Francisco, CA*. http://esl.eslwin.tamu.edu/digital-library.html.

NCDC. 2009. Quality controlled climatological data. National Climatic Data Center, National Satellite and Information Service, U.S. Department of Commerce, Silver Spring, MD. http://cdo.ncdc.noaa.gov/ulcd/ULCD.

NETL. 2008. 2008 Buildings energy data book, November 2008. National Energy Technology Laboratory, U.S. Department of Energy, Energy Efficiency and Renewable Energy, Building Technologies Program, Silver Spring, MD. http://btscoredatabook.eren.doe.gov.

Natural Resources Canada. 2004. Technical fact sheet: Premium-efficiency motors. Report M144-21/2003E, Office of Energy Efficiency, Energy Innovators Initiative, Ottawa, Canada. http://oee.nrcan.gc.ca/Publications/infosource/Pub/ici/eii/pdf/M144-21-2003E.pdf.

Okada, T., Y. Seshimo, T. Yoshikawa, and H. Igarashi. 1992. Research and development of a home use VAV air-conditioning system. *ASHRAE Transactions* 98(2):133-39.

Pang, X., B. Zheng, and M. Liu. 2006. Case study of Continuous Commissioning® in an office building. *Proceedings of the* 6th *International Conference for Enhanced Building Operations, Shenzhen, China*. http://esl.eslwin.tamu.edu/digital-library.html.

Rishel, J.B. 2003. How to calculate motor efficiency for variable-speed centrifugal pumps. *Engineered Systems* 20(8):68-73.

Rose, J.R., and W.L. Kopko. 1994. A novel method for resetting duct static pressure for variable air volume systems. *Proceedings of the 1994 American Council for an Energy-Efficient Economy Summer Study on Energy Efficiency in Buildings, Pacific Grove, CA,* pp. 5:219-223.

Salsbury, T.I., and A. Singhal. 2003. Control system commissioning for enhanced building operations. *Proceedings of the 3rd International Conference for Enhanced Building Operations, Berkeley, CA*. http://esl.eslwin.tamu.edu/digital-library.html.

Song, L., I. Joo, D. Dong, M. Liu, J. Wang, K. Hansen, L. Quiroz, and A. Swiatek. 2003. Optimizing HVAC control to improve building comfort and energy performance. *Proceedings of the 3rd International Conference for Enhanced Building Operations, Berkeley, CA*. http://esl.eslwin.tamu.edu/digital-library.html.

Stum, K. 1998. Using energy management control systems for HVAC operational diagnostics. *Proceedings of the 11th Annual Symposium on Improving Building Energy Efficiency in Hot and Humid Climates, Ft. Worth, TX.* http://esl.eslwin.tamu.edu/digital-library.html.

Taylor, S.T. 2007. Increasing efficiency with VAV system static pressure setpoint reset. *ASHRAE Journal* 49(6):24-32.

Trane. 1991. VAV system optimization: Critical zone reset. Trane Engineers Newsletter 20(2), Trane Inc., La Crosse, WI. http://www.trane.com/commercial/library/EN20-2.pdf.

Trane. 2008. TRACE™ 700, Version 6.2. Trane Inc., La Crosse, WI.

TSI. 2006. VelociCalc® plus air velocity meter, operation and service manual. Report 1980321, Revision H, Trust. Science. Innovation, Shoreview, MN. http://www.tsi.com/uploadedFiles/Product_Information/Literature/Manuals/1980321H-8384-86.pdf.

TSI. 2007. AccuBalance® air capture hoods. Trust. Science. Innovation, Shoreview, MN. http://www.tsi.com/uploadedFiles/Product_Information/Literature/Spec_Sheets/5001004-8371-72-73-AccuBalance.pdf.

Tung, D.S.L., and S. Deng. 1997. Variable-air-volume air-conditioning system under reduced static pressure control. *Building Services Engineering Research & Technology* 18(2): 77-83.

Turner, W.D., S. Deng, J. Hood, M. Butler, and R.K. Pratt. 2003. Continuous Commissioning® of the Matheson courthouse in Salt Lake City, Utah. *Proceedings of the 3rd International Conference for Enhanced Building Operations, Berkeley, CA*. http://esl.eslwin.tamu.edu/digital-library.html.

U. S. Department of Energy. 2005. Energy tips – Motor systems: Motor systems tip sheet #5. Report DOE/GO-102005-2060, U.S. Department of Energy, Industrial Technologies Program, Washington, DC. www1.eere.energy.gov/industry/bestpractices/pdfs/replace_vbelts_motor_systemts5.pdf.

Wang, S., and J. Burnett. 1998. Variable-air-volume air-conditioning systems: Optimized static pressure setpoint. *Building Services Engineering Research & Technology* 19(4):219-31.

Wang, S. 1999. Dynamic simulation of building VAV air-conditioning system and evaluation of EMCS on-line control strategies. *Building and Environment* 34(6):681-705.

Warren, M., and L.K. Norford. 1993. Integrating VAV zone requirements with supply fan operation. *ASHRAE Journal* 35(4):43-46.

Wei, G., D.E. Claridge, Y. Sakurai, and M. Liu. 2000. Improved air volume control logic for VAV systems. *Proceedings of the 12th Annual Symposium on Improving Building Energy Efficiency in Hot and Humid Climates, San Antonio, TX.* http://esl.eslwin.tamu.edu/digital-library.html.

Wei, G., M. Liu, and D.E. Claridge. 2004. Integrated damper and pressure reset for VAV supply air fan control. *ASHRAE Transactions* 110(2):309-13.

Westphalen, D., and S. Koszalinski. 1999. Energy consumption characteristics of commercial building HVAC systems, volume II, thermal distribution, auxiliary equipment, and ventilation. Arthur D. Little, Inc., Cambridge, MA. http://www.commercialbuildinginspections.net/downloads/hvac_energy_consumption_thermal_distribution.pdf.

Wu, L., M. Liu, G. Wang, and X. Pang. 2007. Integrated static pressure reset with fan airflow station in dual-duct VAV system control. *Proceedings of the Energy Sustainability Conference 2007, Long Beach, CA*, pp. 441-49.

Zheng, K., H. Li, and H. Yang. 2007. Application of wireless sensor network (WSN) technologies in optimal static pressure reset in variable air volume (VAV) system. *Proceedings of the 7th International Conference for Enhanced Building Operations, San Francisco, CA*. http://esl.eslwin.tamu.edu/digital-library.html.

Zhu, Y., C. Culp, D. Turner, B. Yazdani, A. Athar, and K. Banks. 2001. Continuous commissioning: A valuable partner to retrofit projects. *Proceedings of the 1st International Conference for Enhanced Building Operations, Austin, TX.* http://esl.eslwin.tamu.edu/digital-library.html.

Zeig, G., G. Wei, W.D. Turner, and J.C. Baltazar-Cervantes. 2007. Continuous Commissioning® of a medical facility. *Proceedings of the 7th International Conference for Enhanced Building Operations, San Francisco, CA*. http://esl.eslwin.tamu.edu/digital-library.html.

APPENDIX A

DUCT MODEL DESCRIPTION

A.1 Air Distribution System Information

The mechanical drawings for JEB were used to model the air distribution system for AHU 5-1. A summary of the main supply duct (non-branch) information used in the model is provided in Table 8.

Table 8. Main supply duct dimensions from building design drawings

Duct Section #	Width (in)	Height (in)	Length (ft)
1	36	36	8
2	24	20	15
3	20	18	30.7
4	20	18	32
5	20	18	2.8
6	20	18	2.45
7	16	14	38.94
8	16	14	3.45
16	20	20	56.6
17	20	20	14
18	18	16	48
19	18	16	21

A field investigation of the branch ducts found them all to be circular flex; however, several discrepancies were found between the installed diameters and those specified in the building design drawings. Consequently, the modeled branch duct diameters were calculated based on the cross-sectional area inputs in the terminal box control programming. A summary of terminal box branch duct dimensions and airflow setpoints are provided in Table 9.

Table 9. Terminal box design and programmed airflow setpoints

Terminal Box	Dia (in)	Length (ft)	Duct Section #	Design* Max/Min (CFM)	As Built** Min/Max (CFM)
FVV-5-1	8.01	4	9	850/255	852/256
VV-5-1	4.28	2	10	125/0	124/0
FVV-5-2	10.04	5	11	970/290	972/292
FVV-5-3	8.01	5	12	620/190	620/192
VV-5-2	4.28	2	13	150/0	152/0
FVV-5-4	8.01	4	14	610/185	800184
FVV-5-5	11.92	3	15	1580/475	1580/476
FVV-5-13	8.01	4	20	525/160	524/160
FVV-5-12	8.01	4	21	665/200	664/200
FVV-5-11	8.01	4.5	22	715/215	716/216
FVV-5-10	14.04	3.5	23	2500/750	2552/752

*From building design drawings
**From terminal equipment controller (TEC) programming

The AHU equipment identified through field investigation is summarized in Table 10. The detailed fan performance data tabulated in Table 11 was obtained from Chicago Blower Corporation (2006) and does not include v-belt losses. The fan outlet area is 3.45 ft^2 and the exact airfoil blade diameter for the installed blower assembly is 17-3/16" (Mikec 2009).

Table 10. Experimental AHU equipment nameplate information

VFD	Manufacturer	Danfoss Graham
	Material	176U2205
	Serial #	039900Y213
	Model	VLT 6000 HVAC
Motor	Manufacturer	Baldor (Super Efficient)
	Catalog #	EM3313T
	Serial #	37F614Y568
	HP	10
	RPM	1760
Fan	Manufacturer	Chicago Blower Corp.
	Serial #	256042-2
	Size	182, Class I
	Model	D51 Double Width Centrifugal Airfoil Fan

Table 11. Blower BHP and RPM data for selected static pressures as a function of airflow

CFM		0.25”	0.38”	0.5”	0.75”	1”	1.25”	1.5”	2”	2.5”	3”
1800	BHP	0.1	0.14	0.18	0.27						
	RPM	541	619	684	813						
2000	BHP	0.11	0.16	0.2	0.29	0.41					
	RPM	563	641	706	821	937					
2500	BHP	0.16	0.21	0.26	0.38	0.49	0.62	0.77			
	RPM	638	696	760	871	962	1055	1148			
3000	BHP	0.23	0.28	0.33	0.47	0.61	0.74	0.88	1.21	1.6	
	RPM	722	772	820	924	1019	1097	1173	1329	1480	
3500	BHP	0.31	0.38	0.44	0.57	0.74	0.91	1.06	1.37	1.74	2.16
	RPM	807	855	897	980	1071	1155	1227	1358	1491	1623
4500	BHP	0.55	0.64	0.72	0.89	1.05	1.22	1.43	1.87	2.27	2.65
	RPM	984	1025	1064	1133	1197	1263	1334	1469	1582	1684
5500	BHP	0.9	1	1.11	1.32	1.53	1.72	1.91	2.36	2.89	3.43
	RPM	1168	1203	1237	1301	1359	1413	1464	1574	1690	1798
6500	BHP	1.39	1.51	1.63	1.88	2.14	2.38	2.62	3.07	3.57	4.15
	RPM	1357	1387	1416	1473	1528	1579	1625	1714	1804	1901
7500	BHP	2.04	2.18	2.32	2.6	2.9	3.19	3.48	4.02	4.54	5.09
	RPM	1548	1574	1600	1651	1700	1748	1793	1876	1953	2029
8500	BHP	2.88	3.03	3.19	3.51	3.84	4.17	4.5	5.16	5.77	6.36
	RPM	1741	1764	1787	1833	1877	1921	1964	2044	2117	2185
9500	BHP	3.94	4.11	4.28	4.63	4.99	5.36	5.73	6.48	7.2	7.9
	RPM	1935	1956	1977	2018	2059	2098	2138	2213	2284	2350
10500	BHP	5.23	5.42	5.61	5.99	6.39	6.78	7.19	8.01	8.84	9.64
	RPM	2130	2149	2169	2206	2243	2280	2316	2386	2454	2518
11500	BHP	6.79	7	7.2	7.62	8.05	8.48	8.91	9.8	10.71	
	RPM	2326	2344	2361	2396	2430	2463	2497	2562	2626	
12500	BHP	8.64	8.86	9.09	9.54	10					
	RPM	2522	2539	2555	2587	2618					

A.2 Experimental AHU Supply Airflow Matrices

$$\mathrm{L} = \begin{Bmatrix} & N_1 & N_2 & N_3 & N_4 & N_5 & N_6 & N_7 & N_8 & N_9 & N_{10} & N_{11} & N_{12} \\ T_1 & 1 & 0 & 0 & 0 & 0 & 0 & 0 & 0 & 0 & 0 & 0 & 1 \\ T_2 & 1 & 1 & 0 & 0 & 0 & 0 & 0 & 0 & 0 & 0 & 0 & 1 \\ T_3 & 1 & 1 & 1 & 0 & 0 & 0 & 0 & 0 & 0 & 0 & 0 & 1 \\ T_4 & 1 & 1 & 1 & 1 & 0 & 0 & 0 & 0 & 0 & 0 & 0 & 1 \\ T_5 & 1 & 1 & 1 & 1 & 1 & 0 & 0 & 0 & 0 & 0 & 0 & 1 \\ T_6 & 1 & 1 & 1 & 1 & 1 & 1 & 0 & 0 & 0 & 0 & 0 & 1 \\ T_7 & 1 & 1 & 1 & 1 & 1 & 1 & 1 & 0 & 0 & 0 & 0 & 1 \\ T_8 & 0 & 0 & 0 & 0 & 0 & 0 & 0 & 1 & 0 & 0 & 0 & 1 \\ T_9 & 0 & 0 & 0 & 0 & 0 & 0 & 0 & 1 & 1 & 0 & 0 & 1 \\ T_{10} & 0 & 0 & 0 & 0 & 0 & 0 & 0 & 1 & 1 & 1 & 0 & 1 \\ T_{11} & 0 & 0 & 0 & 0 & 0 & 0 & 0 & 1 & 1 & 1 & 1 & 1 \end{Bmatrix} \tag{A.1}$$

$$\mathrm{Q_{term}} = \begin{Bmatrix} & \text{Flow} \\ T_1 & \dots \\ T_2 & \dots \\ T_3 & \dots \\ T_4 & \dots \\ T_5 & \dots \\ T_6 & \dots \\ T_7 & \dots \\ T_8 & \dots \\ T_9 & \dots \\ T_{10} & \dots \\ T_{11} & \dots \end{Bmatrix} \tag{A.2}$$

APPENDIX B

FIELD MEASUREMENT INSTRUMENTATION

The system airflow was measured using an air velocity meter (TSI 2006) (Figure 17) and the zonal airflow was measured using a flow hood (TSI 2007) (Figure 18). The air velocity meter was also used to measure the static pressure and both of these instruments are calibrated annually. Detailed measurement specifications for this equipment are provided in Table 12 and Table 13. The blower and motor shaft speeds were measured using a handheld tachometer (Monarch 2009) detailed in Table 14.

Figure 17. Air velocity meter (TSI 8386A)

Figure 18. Air capture hood (TSI 8372)

Table 12. VelociCalc® Plus air velocity meter (TSI 8386A)

	Velocity from a pitot tube (ft/min)	Velocity from thermal sensor (ft/min)	Temp (˚F)	Relative Humidity (RH)	Pressure (inWG)
Range	250 to 15,500	0 to 9,999	14 to 140	0 to 95%	-5 to 15
Accuracy	±1.5% at 2000	±3% of reading or ±3	±0.5	±3%	±1% of reading ±0.005 ±0.02%/˚F
Resolution	1	1	0.1	0.1%	0.001
Response Time	200 msec	200 msec	2 min*	<1 min*	0.1 msec

*66 % of final value

Table 13. AccuBalance® air capture hood (TSI 8372)

Range	30 to 2,000
Accuracy	±5% of reading and ±5
Resolution	1

Table 14. Monarch Pocket-Tach Plus

Range	2.5 to 100,000
Accuracy	Non-contact: ±0.01% of reading Contact: ±0.5% of reading
Resolution	1
Response Time	Twice per second

APPENDIX C

ISSUES IMPACTING SPR PERFORMANCE

The power requirements corresponding to OptSPR were modeled using the hourly averaged 15 minute trended data. Figure 19 was used to identify terminal boxes FVV 5-1 and FVV 5-4 for further analysis.

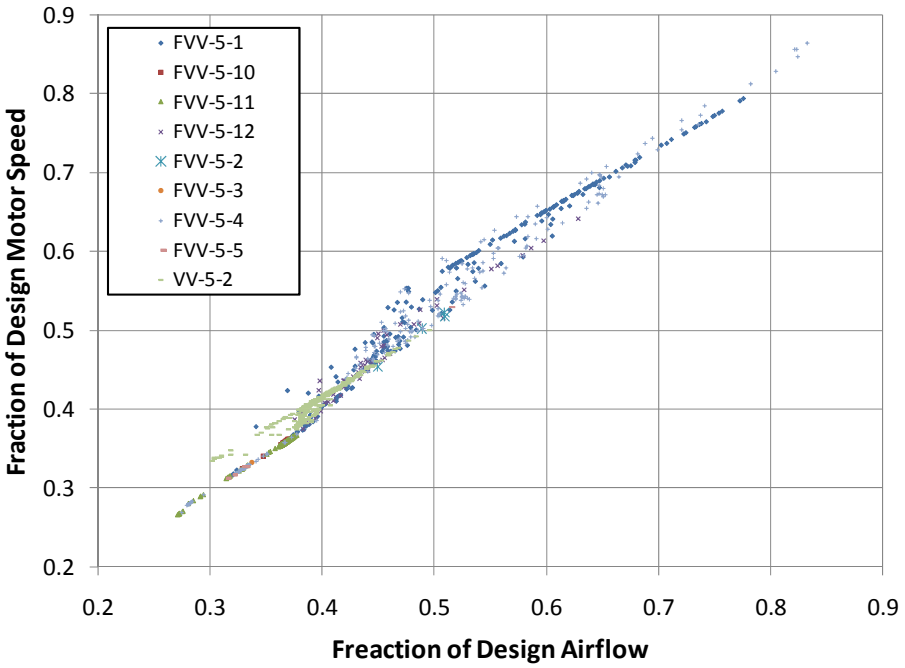

Figure 19. Fraction of design motor speed required during OptSPR control using hourly averaged 15 minute trend airflow data broken down by the terminal box driving the reset from November to February

To ensure that the behavior exhibited in Figure 19 was not exclusive to the duct layout found at JEB AHU 5-1, the model was modified to neglect the terminal boxes supplied by the branch not containing the static pressure sensor. This had the effect of converting the supply duct system into a single main duct serving seven terminal boxes.

C.1 Impact of Maximum Airflow Setpoint

The data points corresponding to FVV 5-4 were investigated to identify the airflow conditions that caused a range of static pressure setpoints to be used for a given system airflow ratio. A review of the terminal box control setpoints for FVV 5-4 led to the discovery that the maximum cooling airflow setpoint had been overridden to 800 CFM. Since the branch duct for this terminal box was sized for 610 CFM, the increase in airflow caused a significantly higher air speed and pressure drop, which led to a higher static pressure requirement. The impact of adjusting the maximum cooling airflow setpoint of FVV 5-4 on SPR performance was investigated using the simplified single duct model and the following airflow adjustment criteria:

IF trended FVV 5-4 airflow > 184 CFM (minimum flow setpoint),
THEN multiply airflow by ratio of design and maximum cooling setpoints (610/800),
ELSE use trended airflow.

It is shown in Figure 20 that the amount of scatter during the time when FVV 5-4 is driving the reset is reduced.

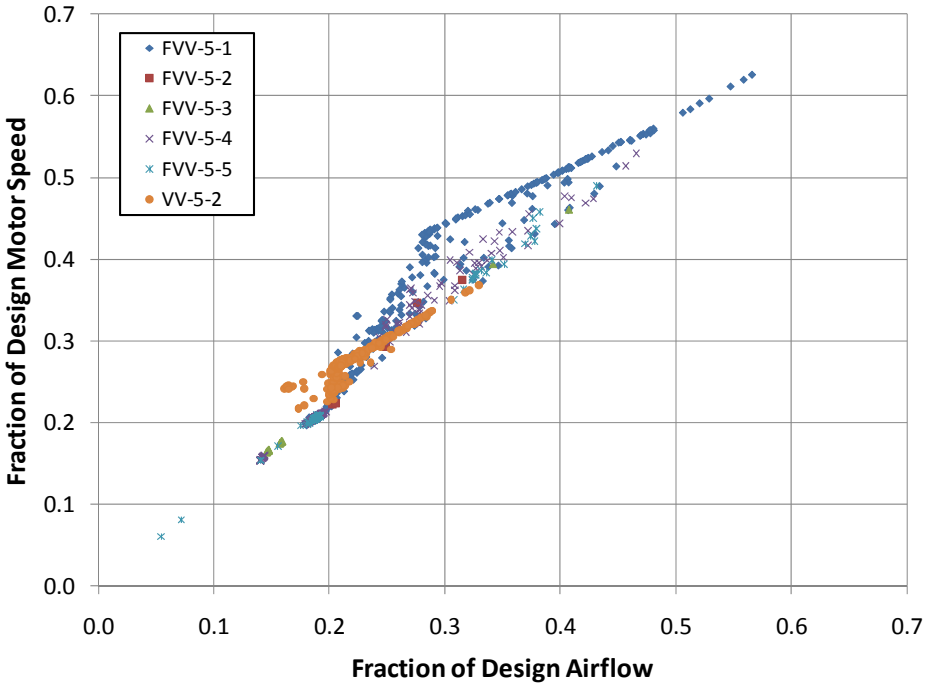

Figure 20. Fraction of design motor speed required during OptSPR control using hourly averaged 15 minute trend airflow data from November to February, while simulating a single main supply duct, broken down by the terminal box driving the reset with adjusted FVV 5-4 airflow trend data

C.2 Impact of Thermostat Reading

An explanation for the pronounced line of points corresponding to terminal box FVV 5-1 was found through a field investigation on March 3, 2009 when SPR control was initially being implemented. This is the closest terminal box to AHU 5-1 and was often at maximum flow continuously during daytime hours. The occupants of this office noted that they were constantly cold. The total airflow measured using a flow hood at each of the diffusers supplied by FVV 5-1 was found to be consistent with the APOGEE maximum airflow setpoint. In addition, the temperature measurement taken at the location of the thermostat matched the APOGEE reading. Once a computer positioned immediately in front of the thermostat was moved, the thermostat reading dropped several degrees and the terminal box damper began to close.

The trended airflows for FVV 5-1 were replaced with modified trended data from FVV 5-2. This procedure takes advantage of the fact that the terminal box thermostats were located in the same corner of the building and the zone usage was identical (graduate student office space with 2-3 occupants and computers). The following criteria was used to adjust the trended FVV 5-2 airflow data:

IF trended FVV 5-1 airflow > 256 CFM (minimum flow setpoint),

THEN multiply FVV 5-2 airflow by ratio of design maximum cooling setpoints (852/972),

ELSE use trended airflow.

Figure 21 shows the combined impact of the changes made to the trended airflows for terminal boxes FVV 5-4 and FVV 5-1.

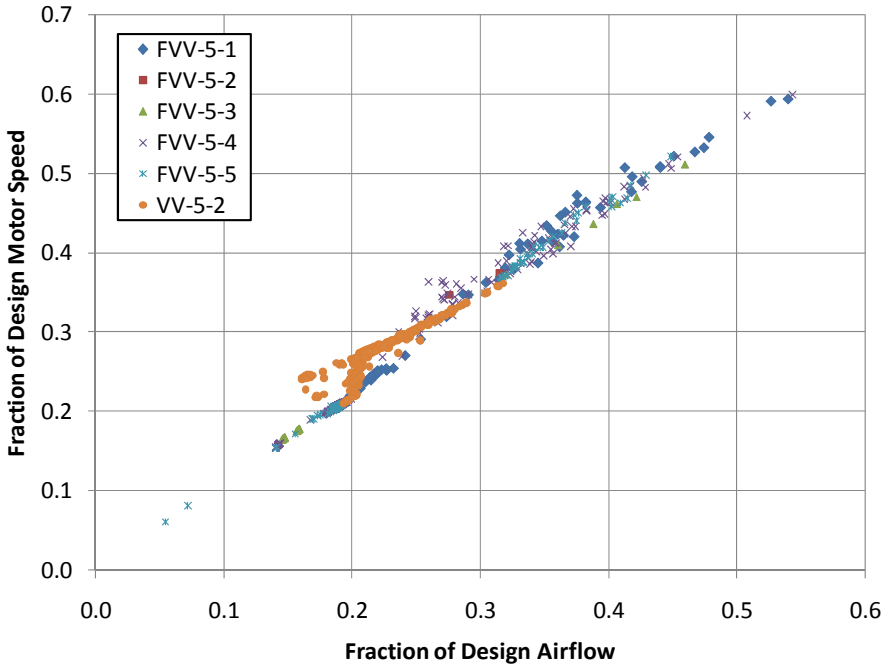

Figure 21. Fraction of design motor speed required during OptSPR control using hourly averaged 15 minute trend airflow data from November to February, while simulating a single main supply duct, broken down by the terminal box driving the reset with adjusted FVV 5-4 and FVV 5-1 airflow trend data

C.3 Impact of System Airflow Distribution on SPR Performance

The system airflow distributions corresponding to the minimum and maximum power requirements at 37% of the design airflow in Figure 21 were examined. Figure 22 illustrates the system airflow conditions, when FVV 5-4 had the highest pressure requirement, and the minimum and maximum static pressure setpoints were 0.359 and 0.599 inWG respectively. Figure 23 illustrates the system airflow conditions, when FVV 5-1 had the highest pressure requirement, and the minimum and maximum static pressure setpoints were 0.424 and 0.752 inWG respectively.

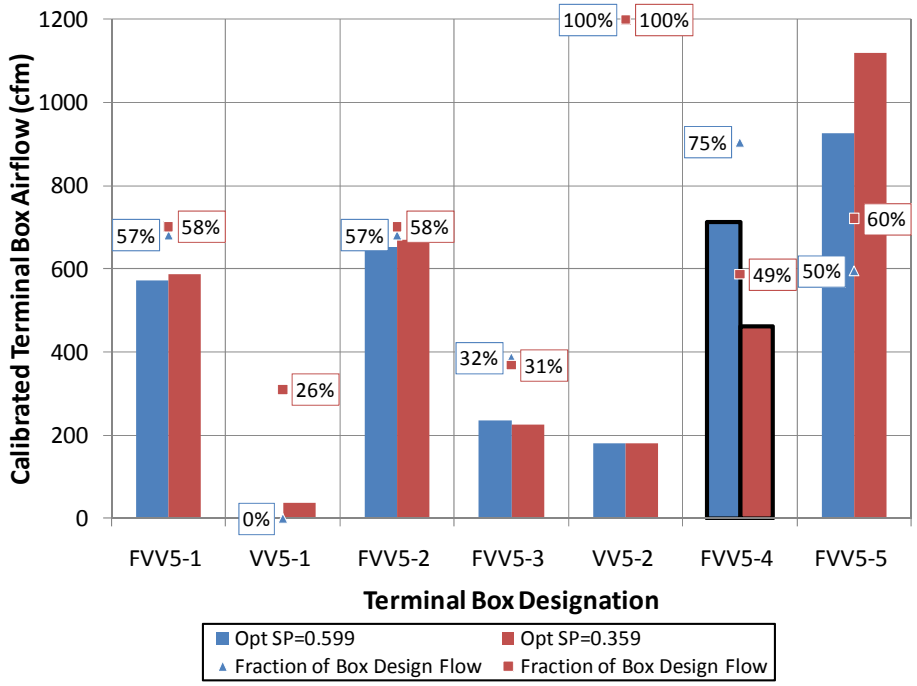

Figure 22. Single duct system flow distribution during 37% system airflow resulting in the minimum and maximum static pressure setpoint selection while FVV 5-4 was driving the reset

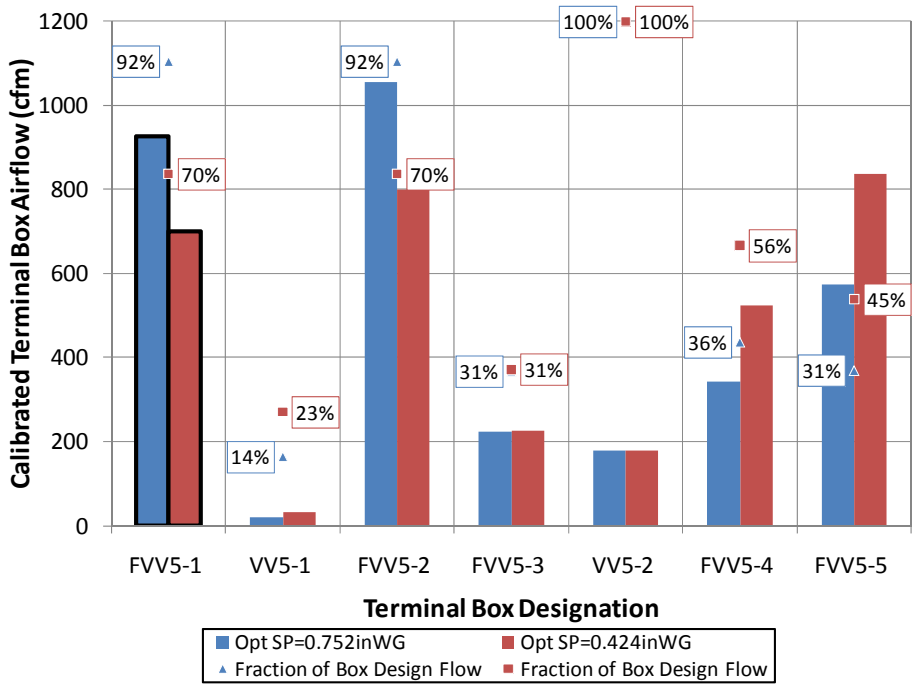

Figure 23. Single duct system flow distribution during 37% system airflow resulting in the minimum and maximum static pressure setpoint selection while FVV 5-1 was driving the reset

It has been shown that while a single terminal box has the highest pressure requirement, the range of static pressure setpoints is directly related to the zonal load ratio. In general, the static pressure setpoints are higher for FVV 5-1 than FVV 5-4 because the zonal load ratios are closer to 100%, which results in a greater frictional pressure drop across the branch duct upstream of the damper.

APPENDIX D

SIMULATING SPR CONTROL WITH EXISTING SOFTWARE

D.1 QuikFan 4.0

This software (EPA 2008) estimates fan power savings from various VSD controls. Fan curves may be specified or selected from a menu that includes: inlet vane, variable pitch, VSD 1/3 reset, and VSD 2/3 reset. The user may modify the existing airflow bin data or create their own by inserting the percentage of hours for each 5% CFM bin.

D.2 Fan System Workbook

This Microsoft Excel based tool (CCC 2008) models the fan energy consumption for a single zone AHU. The user has the ability to input fan curve information, or use the default curve, as well as input detailed system static pressure measurements. This software simulates a zonal demand based SPR by iteratively solving for the static pressure setpoint that will cause the damper to be 100% open.

D.3 TRACE® 700

This commercial software simulates a zonal demand based SPR referred to as the critical zone reset method. This strategy is explained as having a single static pressure sensor located near the fan discharge and a controller to adjust the setpoint based on the position of the critical VAV terminal box damper. Conceptually, this approach has the effect of continuously moving the static pressure sensor to a position immediately upstream of the terminal box with the highest load (Trane 1991; Trane 2008)

VITA

Name: John William Kimla

Address: Energy Systems Laboratory,
MS 3581 Texas A&M University,
College Station, TX 77843

Email Address: jkimla@gmail.com

Education: B.S., Mechanical Engineering, Texas A&M University, 2007
M.S., Mechanical Engineering, Texas A&M University, 2009